General response

We were happy to see that the reviewers found the proposed test case useful for model developers. We appreciate the reviewers' comments and found their suggestions helpful in making our proposed test case even more useful. We address all their comments below and have already implemented most of their suggestions in a revised manuscript. Having said that, we are unable to meet the journal's standards with regard to the supplied codes (e.g. "reference implementation") at this time. Our original intent in submitting the codes for computing the initial conditions was to provide a "first aid" rather than a "commercial grade" software package. The code essentially evaluates algebraic relations that describe the initial (u, v, Φ) fields and requires about 150 lines of code to do so. Evidently, the developers can write the required code better than us and do it in a way that better suits their particular needs, e.g. unstructured meshes. Therefore, we will not include the Fortran and Python codes in the assets of the paper and leave the Matlab code only for the sake of reproducibility. We will accept the editor's decision on this matter. In light of the referees' overall favorable reviews, and our efforts to accommodate their suggestions, we hope that manuscript is accepted for publication in GMD.

Following the reviewers' suggestions (see below), we have implemented the changes summarized below in the revised manuscript.

Added subsections in the Results section:
1. A demonstration of the applicability of the test case to a global-scale model (GFDL, RSW model).
2. An examination of the stability of the waves along the lines used in Thuburn and Li (2000).
3. A demonstration of the use of the proposed test case a linear convergence test (Ref. 1).

Removed items:
1. The H=0.5 m waves were removed. The results of the simulations with this value were less robust. In addition, adhering to a single value of H simplifies the test case.

Replaced items:
1. The spectral analyses were found to be too sensitive to be used for assessment purposes and were therefore replaced with the difference between the global means, which unlike the L2 norm employed by Williamson et al (1992) is insensitive to phase speed errors.

Response (in blue) to the referees' comments (in black)

Anonymous referee #1

General comments:

The Rossby-Haurwitz wave described in test case 6 of Williamson et. al. (1992) is known to be problematic. Thuburn and Li (2000) describes these issues and I think that paper should be referenced here, as it was in the previous paper (Shamir and Paldor, 2016).

The findings of Thuburn and Li (2000) on the Rossby-Haurwitz wave are discussed in the revised Introduction. In addition, we added a new subsection to the Results section, where we examine the generation of small-scale features and the stability of the proposed test case, similar to the way it is done in Thuburn and Li (2000).

One issue is that the original initial conditions as specified in Williamson et. al. (1992) lead to wrapping up of potential vorticity contours and the associated generation of small scale features and potential enstrophy cascade. A figure showing the potential vorticity at several times throughout the simulations would be appreciated here to show that this does not happen for this test case.

For the small wave amplitude, A=1e-5 ms^{-1}, used in our test case the potential vorticity is dominated by the planetary vorticity. Therefore, we added Hovmöller diagrams of the relative vorticity, instead of the potential vorticity, which show that there is no generation of small-scale features during the last wave-period of the simulation. See new section 4.3 and 4^{th} columns in new Figs 1,2,4,5,7 and 8.

The other issue with the original test case is that it is unstable. This is demonstrated numerically in Thuburn and Li (2000) by adding some small noise to the initial conditions after they noticed that the solution they computed using a finite volume model on a grid of hexagons and pentagons (i.e. their only non latitude-longitude model) broke down. The errors related to the structure of the underlying grid triggered the dynamical instability. The solutions in this paper have been computed using a regular latitude-longitude grid so I wonder if a similar issue could occur with this test case. I suggest that the authors could check this by either adding some noise to the initial conditions, as in Thuburn and Li (2000), or by running their code on a rotated grid (i.e. with the poles in the midlatitudes).

Similar to Thuburn and Li (2000) we added a small (5% in our MS) uniformly distributed random noise (perturbation) to the initial conditions (IC). The simulations with the perturbed IC demonstrate that after 100 wave-periods the simulated solutions preserve the initial wave structure. In particular, the small-scale features in the initial u, v, Φ and ξ fields smooth out and do not generate smaller-scale features. See new section 4.3.

some papers use the Rossby wave test as a convergence test, using a reference solution from either a higher resolution run or from a different model. Could the analytical solution here be used to test the convergence of a linear shallow water model? This would provide a useful test in between the steady state test case 2 and the other tests that require a reference solution from a higher resolution run.

We added a convergence test of the linear shallow water model, which demonstrates that the “error” decreases “exponentially” as the resolution increases. Following one of the other comments by the

reviewer on the sensitivity of the spectral analyses we adopted a different assessment criterion which is also used to estimate the error here. See the revised section 3.2 and new section 4.4.

Also, if the wave is indeed stable it would be a fantastic replacement for test case 6, especially for unstructured grid models, or models that use adaptive mesh refinement, since truncation errors related to mesh topology will have no dynamic instability to trigger.

We hope that the revised version of the manuscript, and, in particular, the addition of noise in section 4.3, is more convincing than the previous version. We, too, view the proposed Matsuno test case as a substitute for test case 6 and hope it is adopted by the community.

Specific comments:

1. pg 4, lines 14-15: I am concerned that different pre-factors lead to less stable solutions - it makes me wonder if the version chosen in this paper is indeed stable to differences in grid alignment.

This is a subtle question. There is no reason why Matsuno's expressions should be more stable. We imagine that the most optimal choice of pre-factors can depend on considerations e.g. the prognostic variables used. For example, it is quite possible that different choices are more optimal for models that use vorticity-divergence. Note also that the different pre-factors originate from the use of the normalized Hermite functions whose amplitudes are bounded (Cramér's inequality), as oppose to the amplitudes of the non-normalized Hermite functions that grow indefinitely as n increases. Thus, for large n we expect Matsuno's expressions to be less stable numerically. On the other hand, for the chosen n=1 it is unclear whether the difference between the two forms has any effect on there dtability. Finally, while the present choice might not be the most optimal, the simulated solutions seem to be stable for 100 wave-periods.

2. Figure 2:

Is there any reason why the Rossby wave with H=0.5 is less regular than the other solutions?

We are unsure but the wave modes of H=0.5 m were deleted altogether from the revised manuscript.

Why do some of the contour plots have white regions when the values have been normalised so should lie in the range [-1, 1]?

As is stated in the figure caption, the fields are normalized on the global maximum at t=0. Therefore, the white regions correspond to times when the field's global extrema temporarily exceed the [-1,1] contour range. In our opinion normalizing on the global maximum at t=0 and keeping the contour range fixed is the better option. We added a clarification in the text in the paragraph discussing Figure 1.

3. Power spectra: Are these at all sensitive to the sampling frequency? My experience is that the spectra can be very sensitive to this but maybe that is for more turbulent simulations.

The reviewer is right. By sub-sampling our results by factors of 2 or 4 (so as to insure there are at least 2.5 samples per wave-period) it was evident that while the power spectra were generally similar, the results can be too sensitive to be used for assessment purposes. Therefore, we adopted a different assessment criterion, which is also simpler than the spectral analyses. See the revised section 3.2.

4. Supplement: The code provided to compute the initial conditions, while appreciated, could be improved. The authors state that the code will compute the analytic fields on arbitrary latitude-longitude grids but they have assumed that these grids are structured. These codes will not work as written for unstructured meshes, which are becoming more common in the community. The test case is much more likely to be used if these codes could be amended (i.e. they return values given a list of latitude-longitude values). In addition to this, there are some unnecessarily confusing aspects of the code. For example, there is no need to capitalise variable names so the radius of the Earth, which is called
a in the paper could be a rather than A in the code. The is especially confusing since there is also an A in the equations described in the paper. It would also make sense to have H as an input parameter, since this can be varied.

Thank you, but we have decided to leave the computation of the initial conditions to the developers that can do it better than us and do it in a way that suits their particular needs, e.g. unstructured meshes.

Technical corrections:

1. Equation 3b: This is different to that in the code matsuno.py (and I think the code is correct).

Equation 3b and the code are consistent and both are correct! Note that, in the Fortran code for example, in addition to the different pre-factor in line 200, the expressions in lines 193-194 are also different from the text. The expressions in the code are obtained from the ones in the text by taking another $(gH)^{0.5}$ factor outside of the square brackets, so that the pre-factors of $\hat{u}$ and $\hat{\Phi}$ both have (gH) in the numerator, but ω in 3b is divided by $(gH)^{0.5}$. This was also flagged by Referee #2. Clearly, the difference between the code and the text is confusing. In the revised manuscript we change 3b to match the expressions in the codes.

2. Equation 3c: I think this is missing a sqrt around the gH.

Again, Equation 3c is correct! Dimensional consideration suggests that the referee's suggestion cannot be correct.

With regard to the last two comments, we have repeated the derivation of the expressions in Equation 3 from scratch and derived the same expressions as in the previous version. Also, we encourage the community to implement the test, including different pre-factors and/or different powers of (gH).

Anonymous referee #2

General comments:

1. The manuscript claims (e.g. at the bottom of page 4) that this test case can be used for tropical-channel shallow water models (as presented in this manuscript) and global-scale models. From the manuscript it is not entirely clear that the test will work for global models due to the use of the equatorial beta-plane approximation in the derivation for e.g. the transformations of (x,y) and the wavenumber k. The modeling community (as a 'customer' of this test case) generally works with global shallow water models and tropical-channel model in spherical geometry are extremely rare. It therefore would have been more valuable (or convincing) to present example solutions for a global shallow water model instead of a tropical-channel model. Can the tropical-channel shallow water model also be configured as a global model to demonstrate that the test case works for the whole sphere? Please provide extended explanations or ideally results from a global model.

We added a new subsection to the Results section where we repeat the simulations using a global-scale model (the GFDL, RSW Model). The equatorial channel model cannot be easily adopted to the entire sphere due to the convergence of longitudinal lines at the poles. Therefore, we used GFDL's global-scale model which is spectral. Please see the new section 4.2.

2. Model developments with regular latitude-longitude grids have become very rare over the last decade. More typical grids are now cubed-sphere, hexagonal or icosahedral grid with built-in grid irregularities. The manuscript states that the solutions of this test case are very stable for at least 10 wave periods, which is demonstrated on a regular lat-lon grid. This triggers the question whether this statement will hold for today's models with non-latitude-longitude grids. Another question is whether small perturbations of the initial conditions will disrupt or shorten the stability of the test case. Please provide information on these aspects.

Unfortunately, we are unable to provide results with a non-latitude-longitude grid model. We hope the community will employ the Matsuno test case with such models and comment on the subject.

With regard to the perturbations, we added a new subsection to the Results section where we examine the stability of the chosen waves. As in Thuburn and Li (2000) we added a small (5% in our MS) uniformly distributed random noise (perturbation) to the initial conditions (IC). The simulations with the perturbed IC demonstrate that after 100 wave-periods the simulated solutions preserve the initial wave structure. In particular, the small-scale features in the initial u, v, Φ and ξ fields smooth out and do not generate smaller-scale features. See new section 4.3.

3. As detailed below (points 5-7), the description of the initial conditions is incomplete. In addition, the analytic equations (Eq.(3)) differ slightly from the implementation in the Fortran, Matlab and Python codes. The test is therefore not usable by others in its current form, and the manuscript/codes need to be corrected.

All the required information can be found in the original manuscript, and Equation (3) and the code are consistent and are both correct! Evidently, the original version was not clear/organized enough. We hope that the revised version does a better job at conveying the information. Please see detailed response to points 5-7 below.

Technical comments:

1. Page 1, line 9, also page 2, line 32: Please describe the model as an 'equatorial channel' model.

We now refer to the model as an 'equatorial channel' model as requested.

2. Page 1 line 12, page 2 line 2, page 5 lines 3&7: Generalize the description of the grids. A test case for only 'latitude-longitude' grids will have rather limited use. I think you meant to say that given the location of a latitude and longitude, the initial conditions and analytic solutions can be computed on any grid.

Fixed

3. Page 2, line 24: It is incorrect to say that the term 'baroclinic' is associated with density variations in the vertical directions. A flow with identical density and pressure variations (e.g. for isothermal conditions) is still barotropic. Density and pressure variations need to vary independently of each other.

Rephrased in the revised version

4. Page 3, line 15: What is meant by 'reduced gravity'. The initialization of the test case uses the regular Earth's gravity. Modify.

The reviewer is right. As stated in page 5, line 24 of the original manuscript, we control the speed of gravity waves $(gH)^{0.5}$ by holding g fixed and equal to the Earth gravitational acceleration and varying H. The use of the term 'reduced gravity' originates from the fact that the linearized shallow water equations can also be derived as the horizontal structure equations in a stratified layer (in the linear case with a motionless mean flow), in which case Earth gravity is replaced by the reduced gravity and

the layer depth by the equivalent height. In order to avoid confusion, we removed these two terms and in the revised manuscript we now adhere to a "single layer" fluid.

5. Page 3, line 17, also page 5&6 section 3.1: The wave mode n=1 is selected which leads to three distinct real roots in Eq. (2). Two of these roots are selected for the example results, but no equations are given for the Rossby wave root and EIG root. Without this information, the description of the initial conditions is incomplete. Add this information to Section 3.1.

This information was provided in Appendix A of the original manuscript. In the revised version this information is moved to the main text after Equation (2) in Section 2, which is more suitable than sec. 3.1.

6. Page 4, Eq. (3) and text: The manuscript fails to explain the meaning and definition of ψ n . What is the relationship between ψ n and the normalized Hermite polynomials H n ? Without the definition of ψ n the description of the initial conditions is incomplete.

ψ_n equals $\hat{v}_n$. Thus, in the revised manuscript we have decided to remove ψ_n altogether and adhere to $\hat{v}_n$, which is just the latitude-dependent amplitude of the meridional velocity.

7. Page 4, Eq. (3): Eq. (3) seems to be correct, but the Fortran/Matlab.Python scripts use a wrong u_hat calculation. E.g. the Fortran code in line 200 needs to read sqrt(g*H0) instead of just 'g*H0'.

Equation 3 and the code are consistent and both are correct! Note that, in the Fortran code for example, in addition to the different pre-factor in line 200, the expressions in lines 193-194 are also different from the text. The expressions in the code are obtained from the ones in the text by taking another $(gH)^{0.5}$ factor outside of the square brackets, so that the pre-factors of $\hat{u}$ and $\hat{\Phi}$ both have (gH) in the numerator, but ω in 3b is divided by $(gH)^{0.5}$. This was also flagged by Referee #1. Clearly, the difference between the code and the text is confusing. In the revised manuscript we change 3b to match the expressions in the codes.
We have repeated the derivation of the expressions in Equation 3 from scratch and derived the same expressions as in the previous version. Also, we encourage the community to implement the test, including different pre-factors and/or different powers of (gH).

8. Page 4, line 10: State that the amplitude A needs to have units of m/s.

Added – Thank you

9. Page 4, line 25: you imply that the planar wavenumber k is unitless, so that that spherical wavenumber k/(a cosφ 0) has units of 1/m. Please comment and clarify.

The planar wave-number has units of 1/length, while the spherical wave-number is dimensionless. To avoid any confusion we added a subscript ‘s’ for spherical variable and a comment in the text.

Correct typo, should be ‘replaced’. Corrected. Thank you

10. Page 8, line 1: What is meant by the ‘transport form’ of the SWEs? This seems to imply the ‘advective form’. However, the provided equations are in ‘conservation form’.

The reviewer is right, the equations are in ‘conservation form’ - corrected.

11. Page 8, line 10: Explicitly state whether the example model uses diffusion or smoothing/filtering operations for the computations, and if yes, which ones. Should users of the test case try to omit all diffusion/filtering operations in their models when using this test case? E.g. the provided shallow water code contains provisions for a temporal Asselin filter.

The equatorial channel model has no diffusion/viscosity terms. It does contain provisions for a Robert-Asselin filter, but in our implementation the coefficient is set to zero. The global model also contains hyperdiffusion terms, but the coefficient was also set to zero. Please see the revised model descriptions. As is stated in the first paragraph of section 3.1, we consider the choice of diffusion/viscosity terms a modeling choice, but we acknowledge the other approach of specifying them as part of the test case.

12. Page 9, Fig. 2: The value for the symbol φ f is not provided. Add this information.

φ_f is removed from the text of the revised version.

13. Page 9, Fig. 2: It is highly unusual and confusing to see and interpret the flipped Hovmoeller diagrams. Typically, Hovmoeller diagrams list the position along the x-axis and time along the y-axis. I recommend flipping the axes in Fig. 2 to make the interpretation of the Hovmoeller diagrams easier.

To conform to common practice we changed the longitude-time diagrams into time-longitude diagrams.

14. Supplemental material: Please add Fortran/Matlab wrapper codes that will enable the user to create/test the initial conditions. In addition, the codes should not expect to receive regular longitude and latitude arrays, but should be callable for any longitude and latitude position.

Thank you, but we have decided to leave the computation of the initial conditions to the developers that can do it better than us and in a way that suits their particular needs, e.g. unstructured meshes.

The Matsuno baroclinic wave test case

Ofer Shamir[1], Itamar Yacoby[1], and Nathan Paldor[1]

[1]Fredy and Nadine Herrmann Institute of Earth Sciences, Edmond J. Safra Campus, Givat Ram, The Hebrew University of Jerusalem, Jerusalem, Israel

Correspondence: Nathan Paldor (nathan.paldor@huji.ac.il)

Abstract. The analytic wave-solutions obtained by ~~Matsuno (1966)~~ Matsuno (1966) in his seminal work on equatorial waves provide a simple and informative way of assessing atmospheric ~~and oceanic~~ models by measuring the accuracy with which they simulate these waves. These solutions approximate the solutions of the shallow water equations on the sphere for small speeds of gravity waves such as those of the baroclinic modes in the atmosphere~~and ocean~~. This is in contrast to the solutions of the non-divergent barotropic vorticity equation, used in the Rossby-Haurwitz test case, which are only accurate for large speeds of gravity waves such as those of the barotropic mode. The proposed test case assigns specific values to the wave-parameters (gravity wave speed, zonal wave-number, meridional wave-mode and ~~amplitude~~wave-amplitude) for both planetary and inertia gravity waves, and ~~confirms the accuracy of the simulation by employing Hovmöller diagrams and temporal and spatial spectra. The proposed test case~~ suggests simple assessment criteria suitable for zonally propagating wave solutions. The test is successfully applied to ~~a standard finite-difference, equatorial , non-linear,~~ both an equatorial channel spherical shallow water model~~in spherical coordinates, which demonstrates that Matsuno's wave-solutions can be accurately simulated~~ , and a global-scale one. By adding a small perturbation to the initial fields it is demonstrated that the chosen initial waves remain stable for at least ~~10~~ 100 wave-periods~~, which for oceanic planetary waves is nearly 1300 days. In order to facilitate the use of the~~ . The proposed test case ~~, we provide Matlab, Python and Fortran codes for computing the analytic solutions at any time on arbitrary latitude-longitude grids~~can also be used as a resolution convergence test.

1 Introduction

A cornerstone of global-scale model assessment is the Rossby-Haurwitz test case, originally used by ~~Phillips (1959)~~ Phillips (1959) as a qualitative way of assessing his shallow water model. Phillips initialized his model with an analytic wave-solution of the non-divergent barotropic vorticity equation obtained by ~~Haurwitz (1940)~~Haurwitz (1940), and examined the spatio-temporal smoothness of the simulated fields at later times. Using this procedure he concluded that the emergent noise in his model was due to a ~~small but significant~~ small-but-significant, divergence field missing from the initial fields. Even though the solutions of the non-divergent barotropic vorticity equation are not solution of the Shallow Water Equations (SWEs), Phillips' procedure was adopted by ~~Williamson et al. (1992)~~ Williamson et al. (1992) as a standard test case for shallow water models and has been

extensively used ever since (Jablonowski et al., 2009; Mohammadian and Marshall, 2010; Bosler et al., 2014; Ullrich, 2014; Li et al., 2015, are only five recent examples).

~~Recently, Shamir and Paldor (2016)~~ However, there are two known issues with the original Rossby-Haurwitz test case that limit its usefulness (Thuburn and Li, 2000). The first is the generation of small-scale features via potential enstrophy cascade, which requires adequate dissipation mechanisms to remove enstrophy at the grid scale (in order to mimic a continuous cascade to sub-grid scales). The second is the instability of the initial wave-number 4 used in the Rossby-Haurwitz test case. In contrast to Hoskins (1973) who found that wave-numbers smaller than or equal to 5 are stable, Thuburn and Li show that Rossby-Haurwitz wave-number 4 is in fact also unstable.

Recently, Shamir and Paldor (2016) proposed a similar procedure to that of Phillips (1959) where ~~,~~ instead of using the solutions of the non-divergent barotropic vorticity equation, the initial fields are ~~taken from~~ the analytic wave-solutions of the linearized SWEs on the sphere ~~obtained by Paldor et al. (2013)~~derived in Paldor et al. (2013). These solutions fully account for the small ~~but significant~~ divergence field and can be ~~evaluated on arbitrary latitude-longitude grids~~computed on any grid given the locations of the latitudes and longitudes. In particular, they include the fast propagating ~~Inertia~~ Inertia- Gravity (IG) waves ~~, which are completely filtered out by~~ that are completely absent from the the non-divergent barotropic vorticity equation. Consequently, the procedure proposed by Shamir and Paldor provides a more quantitative assessment than Phillips's original procedure ~~, and~~ though it is just as easy to implement.

Both solutions obtained by ~~Haurwitz (1940)~~ Haurwitz (1940) and Paldor et al. (2013) approximate the solutions of the SWEs in the asymptotic limit of large speed of gravity waves. For most practical purposes they are sufficiently accurate for speeds of gravity waves of about $200-300$ ms^{-1} or higher, which are typical of the barotropic mode in Earth's atmosphere and oceans. However, typical speeds of gravity waves of baroclinic modes ~~are about $20-30$ ms^{-1} for~~ in the (tropical) atmosphere ~~(Wheeler and Kiladis, 1999) and $2-3$ ms^{-1} for the oceans (Chelton et al., 1998)~~are about $20-30$ ms^{-1} (Wheeler and Kiladis, 1999). Thus, the above procedures are only relevant for assessing the accuracy with which the barotropic wave mode is ~~resolved~~simulated. In order to assess the accuracy of the baroclinic wave modes we propose, in the present work, to use the analytic wave-solutions of the linearized SWEs on the equatorial β-plane obtained by ~~Matsuno (1966), which~~ Matsuno (1966) that approximate the solutions of the SWEs on the sphere in the asymptotic limit of small speed of gravity waves (De-Leon and Paldor, 2011; Garfinkel et al., 2017).

In addition to being on two opposite ends of the spectrum ~~in terms of the relevant speeds~~ of gravity wave ~~,~~ speed the solutions obtained by ~~Matsuno (1966)~~ Matsuno (1966) differ from those obtained by both ~~Haurwitz (1940) and Paldor et al. (2013)~~ Haurwitz (1940) and Paldor et al. (2013) in their meridional extent. ~~The former become negligible~~ While the former become negligibly small outside a narrow equatorial band ~~, whereas~~ the latter two have non-negligible amplitudes in the vicinity of the poles. Thus, while the Rossby-Haurwitz test case is only relevant to global-scale models, the test case proposed in the present study is applicable to both global-scale and tropical models.

A homonymous, but unrelated, test case is the baroclinic wave test case developed in ~~Jablonowski (2004) and Jablonowski and Williamso~~ Jablonowski (2004) and Jablonowski and Williamson (2006) and independently in ~~Polvani et al. (2004)~~Polvani et al. (2004), and its variants in ~~Lauritzen et al. (2010) and Ullrich et al. (2014)~~Lauritzen et al. (2010) and Ullrich et al. (2014). This test case

is concerned with the non-linear generation of synoptic-scale eddies in multi-layer models via baroclinic instability. In contrast, the ~~proposed test case~~ test case proposed here is concerned with linear wave propagation in (non-linear) single-layer models. ~~While the customary use of~~ In particular, while the term baroclinic ~~is associated with density variations in the vertical direction, here the same~~ usually implies the use of multi-layer models, here this term is used to denote ~~thin layers of fluid~~ single layer model of homogeneous density where the gravity waves speeds are similar to those observed in baroclinic modes in the atmosphere~~and oceans~~.

The idea of using Matsuno's solutions as a test case in a similar fashion to that of the Rossby-Haurwitz test case is most likely not original, but has never been standardized. Thus, the purpose of the present work is to standardize the Matsuno test case in the same spirit that ~~Williamson et al. (1992)~~ Williamson et al. (1992) standardized the Rossby-Haurwitz one. We start with a short description of the analytic expressions derived by ~~Matsuno (1966)~~ Matsuno (1966) in section 2. The proposed test procedure, including the choice of wave-parameters and assessment criteria, is described in Section 3. ~~We then~~ In section 4 we demonstrate the usefulness of the proposed test case ~~in section ??, using a standard finite-difference, equatorial , (non-linear)~~ using both an equatorial channel spherical shallow water model~~in spherical coordinates~~, and a global-scale one. In addition, we examine the smoothness and stability of the initial waves in a similar fashion to that used in Thuburn and Li (2000) and demonstrate the possibility of using the proposed test case as a resolution convergence test. The paper ends with some concluding remarks in section 5.

2 The analytic solutions

The proposed test case is based on the analytic solutions of the SWEs on the equatorial β-plane obtained by ~~Matsuno (1966)~~ Matsuno (1966). These solutions have the form of zonally propagating waves, i.e.

$$\begin{bmatrix} u(x,y,t) \\ v(x,y,t) \\ \Phi(x,y,t) \end{bmatrix} = \begin{bmatrix} \hat{u}(y) \\ \hat{v}(y) \\ \hat{\Phi}(y) \end{bmatrix} e^{i(kx-\omega t)} \tag{1}$$

where x and y are the local Cartesian coordinates in the zonal and meridional directions, respectively; t is time; u and v are the velocity components in the zonal and meridional directions, respectively; Φ is the geopotential height; k is the planar zonal wave-number (which has dimensions of m^{-1}); ω is the wave-frequency; and $\hat{u}(y), \hat{v}(y)$ and $\hat{\Phi}(y)$ are the latitude dependent amplitudes. In accordance with the sign convention used in Matsuno we assume k is non-negative and let ω take any real value. Note, however, that the sign in front of ω in (1) is opposite to that in Matsuno's theory. The convention chosen here is more intuitive as it implies that positive values of ω correspond to waves that propagate in the positive x direction, i.e. ~~in the eastwarddirection~~eastward.

The unknown wave-frequencies and latitude dependent amplitudes are derived from the (well-known) energies and eigenfunctions of the (time-independent) Schödinger equation of ~~the~~ quantum harmonic oscillator. The resulting frequencies are

given by the solutions of the following cubic equation

$$\omega_{n,k}^3 - \left[gHk^2 + \frac{2\Omega\sqrt{gH}}{a}(2n+1)\right]\omega_{n,k} - \frac{2\Omega gHk}{a} = 0, \tag{2}$$

for $n = -1, 0, 1, 2, \ldots$, where Ω ~~and~~ , a and g are Earth's angular frequency ~~and~~ , mean radius, ~~respectively; g~~ and gravitational acceleration respectively; and H ~~are the reduced gravity and equivalent~~ is the layer's depth.

For $n \geq 1$ Equation (2) has three distinct real roots corresponding to a slowly westward propagating Rossby wave, a fast Eastward propagating Inertia Gravity (EIG) wave, and a fast Westward propagating Inertia Gravity (WIG) wave. For $n = 0$ one of the three roots, the one corresponding to a westward propagating gravity wave with $\omega = -\sqrt{gH}k$, leads to infinite zonal wind and is thus discarded as a physically reasonable solution. The remaining two roots correspond to the lowest (i.e. $n = 0$) EIG wave and the Mixed Rossby-Gravity (MRG) wave. For $n = -1$ Equation (2) has one real root $\omega = \sqrt{gH}k$, which correspond to the equatorial Kelvin wave (see Matsuno, 1966). The existence of the latter two waves on a sphere is discussed in Garfinkel et al. (2017) and Paldor et al. (2018)

For given values of the zonal wave-number, k, and meridional mode-number, n, the roots of the cubic equation can be obtained in a closed analytic form using the solutions of the general cubic equation as follows (e.g. Abramowitz and Stegun, 1964) :

$$\omega_{n,k,j} = -\frac{1}{3}\left(\Delta_j + \frac{\Delta_0}{\Delta_j}\right), \quad \text{for} \quad j = 1, 2, 3 \tag{3}$$

where j stands for the three roots, and where

$$\Delta_0 = 3\left[gHk^2 + \frac{2\Omega\sqrt{gH}}{a}(2n+1)\right], \tag{4a}$$

$$\Delta_j = \left[\frac{\Delta_4 + \sqrt{\Delta_4^2 - 4\Delta_0^3}}{2}\right]^{1/3} \exp\left(\frac{2\pi j}{3}i\right), \tag{4b}$$

$$\Delta_4 = -\frac{54\Omega gHk}{a}. \tag{4c}$$

Given the definitions in (4), the explicit expressions for the frequencies of the Rossby, WIG and EIG waves are obtained by sorting the values in (3) as follows:

Rossby :
$$\omega_{n,k,\mathrm{R}} = -\min_{j=1,2,3}|\omega_{n,k,j}|, \tag{5a}$$

Westward Inertia-Gravity :
$$\omega_{n,k,\mathrm{WIG}} = \min_{j=1,2,3}\omega_{n,k,j}, \tag{5b}$$

Eastward Inertia-Gravity :
$$\omega_{n,k,\mathrm{EIG}} = \max_{j=1,2,3}\omega_{n,k,j}. \tag{5c}$$

Having found (one of) the wave-frequencies for a given combination of n and k, the corresponding latitude dependent amplitudes can be written as

$$\hat{v}_n = \psi A H_n \left[\epsilon^{1/4}\left(\frac{y}{a}\right)\right] \exp\left[-\frac{1}{2}\epsilon^{1/2}\left(\frac{y}{a}\right)^2\right] \tag{6a}$$

$$\hat{u}_{n,k} = \frac{\sqrt{gH}\epsilon^{1/4}}{ia(\omega_{n,k}^2 - gHk^2)} \frac{gH\epsilon^{1/4}}{ia(\omega_{n,k}^2 - gHk^2)} \left[-\sqrt{\frac{n+1}{2}}\left(\omega_{n,k}\frac{\omega_{n,k}}{\sqrt{gH}} + \sqrt{gH}k\right)\psi\hat{v}_{n+1} - \sqrt{\frac{n}{2}}\left(\omega_{n,k} - \sqrt{gH}k\frac{\omega_{n,k}}{\sqrt{gH}} - k\right)\psi\hat{v}_{n-1}\right] \tag{6b}$$

$$\hat{\Phi}_{n,k} = \frac{gH\epsilon^{1/4}}{ia(\omega_{n,k}^2 - gHk^2)} \left[-\sqrt{\frac{n+1}{2}}\left(\omega_{n,k} + \sqrt{gH}k\right)\psi\hat{v}_{n+1} + \sqrt{\frac{n}{2}}\left(\omega_{n,k} - \sqrt{gH}k\right)\psi\hat{v}_{n-1}\right], \tag{6c}$$

for $n = 1, 2, 3, \ldots$ (the cases $n = -1, 0$ require special treatment), where

$$\psi_n = AH_n\left[\epsilon^{1/4}\left(\frac{y}{a}\right)\right]\exp\left[-\frac{1}{2}\epsilon^{1/2}\left(\frac{y}{a}\right)^2\right].$$

~~Here~~ $\epsilon = (2\Omega a)^2/gH$ is Lamb's parameter, A is an arbitrary amplitude (that has dimensions of m s^{-1}), and $\hat{H}_n$ are the normalized Hermite polynomials of degree n. Note: (i) The chosen normalization for the latitude dependent amplitudes in (6) is different from the one used in Matsuno. We use the above normalization for convenience, as it ~~relates the amplitude of~~ guarantees that $\hat{v}$ ~~to that of ψ in a straight forward way and guarantees that it~~ is independent of both k or ω. (ii) The use of the normalized version of the Hermite polynomials also leads to slightly different pre-factors in front of ~~ψ_{n+1} and ψ_{n-1}~~ $\hat{v}_{n+1}$ and $\hat{v}_{n-1}$ compared to Matsuno. However, they are generally more stable ~~and more convenient for the spectral analyses employed in the following sections~~.

While the solutions obtained by ~~Matsuno (1966)~~ Matsuno (1966) apply for the equatorial β-plane, the proposed test case is intended for use in spherical models. As is shown in ~~Garfinkel et al. (2017)~~Garfinkel et al. (2017), the SWEs on the equatorial β-plane approximate the SWEs on the sphere to zero-order in powers of $1/\epsilon^{1/4}$. Thus, the solutions obtained by Matsuno are only accurate in the asymptotic limit $\epsilon \to \infty$. For the fixed values of Earth's angular frequency and mean radius, this implies that the solutions obtained by Matsuno are only accurate for sufficiently small speeds of gravity waves $\sqrt{gH}$.

In practice, in order to use Matsuno's solutions in spherical models, the local Cartesian coordinates x and y in the above formulae (1) and (6) have to be replaced by the longitude λ and latitude ϕ of the geographical coordinate system. Recall that the transformation ~~between the two system~~ from the Cartesian system to the spherical one is $(x, y) \to a(\cos\phi_0\lambda, \phi)$, where ϕ_0 is the central latitude ~~to which the β-plane~~ where the planar approximation is applied. ~~Thus, for the equatorial β-plane where $\phi_0 = 0$, the transformation is simply $(x, y) \to a(\lambda, \phi)$.~~ Likewise, the planar ~~wavenumber~~ wave-number k in all of the formulae (1)-(6) has to be ~~replace~~ replaced by its spherical counterpart, k_s, using the transformation ~~$k \to k/a\cos\phi_0 = k/a$.~~

~~For the small gravity wave speeds (i.e. small values of ϵ) used in the present work, the eigenfunctions in become negligible outside a narrow equatorial band (see Sections 3.1 and ?? below). Thus, the above expression can be used to test both~~

~~global-scale and tropical models~~$k \to k_s/a\cos\phi_0$. Thus, for the equatorial β-plane where $\phi_0 = 0$, the transformation is simply $(x, y) \to a(\lambda, \phi)$ and $k \to k_s/a$. In particular, the reader should note that the planar wave-number k has units of m^{-1} while the spherical wave-number k_s is dimensionless.

Finally, using the above formulae to calculate the waves' ~~frequencies and~~ latitude dependent amplitudes requires routines for ~~finding the roots of the cubic equation , and for~~ evaluating the normalized Hermite polynomials on ~~arbitrary latitude-longitude grids. The roots of the cubic equation can be obtained in a closed analytic form using the solutions of the general cubic equation as detailed in appendix **??**. The normalized Hermite polynomials, in turn, can be evaluated using their~~ any grid given the locations of the latitudes. This can be done using the Hermite three-term recurrence relation, as in ~~Press et al. (2007). In order to facilitate the application of the proposed test case we provide as part of the online supplementary material Matlab, Python and Fortran codes (named matsuno.m, matsuno.py and matsuno.f90, respectively) for computing the analytic fields on arbitrary latitude-longitude grids~~Press et al. (2007).

3 Proposed test procedure

The general procedure of the proposed test case is similar to the Rossby-Haurwitz one in that the model in question is initialized with velocity and height fields corresponding to a particular wave-solution and the time evolution of that wave is then examined. The initial wave fields in this case are taken from the analytic expressions in Section 2. The specific choice of wave-parameters and assessment criteria in the present work are discussed below, separately. As is often the case, these choices represent compromises between conflicting factors, e.g. adherence to observations vs. adherence to asymptotic validity of the analytic solutions or rigorous testing vs. simplicity. In any case, these choices may be the subject of discourse as deemed appropriate by the community.

3.1 wave-parameters

The wave-parameters consist of the speed of gravity waves $\sqrt{gH}$, the wave-number and wave-mode k and n, the wave-amplitude A, and the wave-type. Any given combination of these parameters completely ~~specify~~ specifies a unique wave using the expressions in (1)-(6). We consider all other parameters, including the spatio-temporal resolution and the form of diffusion/viscosity terms, to be modeling choices left to the developers. This approach is aimed at testing the models in their modus operandi. However, as noted in ~~Polvani et al. (2004)~~Polvani et al. (2004), different choices for the form of diffusion/viscosity terms correspond to different sets of equations and may not converge to the same solutions.

~~We offer two different choices for~~ The choice of gravity wave speed $\sqrt{gH}$ is inspired by the observed ~~speeds~~ speed of gravity waves of the baroclinic modes in the atmosphere~~and oceans~~. In practice we keep g fixed to Earth's gravitational acceleration, and ~~vary~~ set the speed of gravity waves by ~~varying H. For atmospheric models we suggest using~~ letting $H = 30$ m, which is within the range of observed equivalent depths in the equatorial atmosphere (Wheeler and Kiladis, 1999). ~~For ocean models we suggest using $H = 0.5$ m, which corresponds to the observed speed of gravity waves of the first baroclinic mode in the oceans (Chelton et al., 1998).~~ As mentioned in section 2, the analytic solutions obtained by Matsuno ~~for~~ on the equatorial β-plane are

only accurate approximations of the SWEs on the sphere in the asymptotic limit of small speeds of gravity waves. The above ~~values were~~ value was found by trial and error to be sufficiently accurate in the sense that ~~they yield stable integrations~~ it yields stable solutions for at least ~~10~~ 100 wave-periods in the simulations ~~demonstrated in Section ??~~described in Section 4.

In addition to the speed of gravity waves, the accuracy of Matsuno's solutions ~~depend~~ depends on the wave-number and wave-mode as well. For a given value of $\sqrt{gH}$, ~~they~~ these solutions become asymptotically accurate in the limits $k, n \to 0$ (but $k \neq 0$) (De-Leon and Paldor, 2011). In addition, the higher the wave-number or wave-mode are, the greater the spatial variability and the required spatial resolution are. Both of these considerations suggest that reasonable choices for the wave-number and wave-mode consist of small to moderate values. The proposed wave-number and wave-mode are $k = 5$ and $n = 1$, ~~which are~~ i.e. within the range of dominant values observed in the equatorial atmosphere (Wheeler and Kiladis, 1999), but other choices may work just as well provided k and n are not too large.

The proposed test case is based on the solutions of the linear SWEs but is intended to be used in non-linear models. Therefore, the waves-amplitude should be sufficiently small so as to satisfy the linearization condition. The proposed amplitude of ~~Equation is $A = 10^{-8}$~~ $\hat{v}$ in Equation (6) is $A = 10^{-5}$ m s^{-1}, chosen by trial and error so as to enable stable ~~integrations~~ solutions for at least ~~10~~ 100 wave periods in the simulations ~~in Section ??~~of Section 4.

In general, there are two qualitatively different wave types, ~~the~~ Rossby and IG wave~~types~~, that differ in the magnitude of their divergence ~~field~~and vorticity fields. The former is more solenoidal (non-divergent), whereas the latter is more irrotational. In order to assess the models' performances in these two qualitatively different limits we suggest using one of each. Since Rossby waves are exclusively westward propagating, we choose the EIG wave ~~from~~ of the two IG waves as the second one ~~in order to eliminate potential longitudinal biases~~to cover the two directions of longitudinal direction.

~~The initial u, v, Φ fields of the Rossby (top row) and EIG (bottom row) waves obtained using the analytic expressions of Section 2 and the parameters of Section 3.1 with $H = 0.5$ m. Each field is normalized on its own global maximum. Contour-levels range from -1.0 to $+1.0$ by 0.2. White dashed-lines (in b and e): intersects used for the Hovmöller diagrams in Figure 2.~~ The resulting wave-periods T for the chosen values of $\sqrt{gH}$, k and n are $T = 18.5$ days for the Rossby wave and $T = 1.9$ days for the EIG wave.

3.2 Assessment criteria

For sufficiently small wave-amplitudes we expect the spatio-temporal structure of the simulated solutions to be that of zonally propagating waves, i.e. ~~$\hat{\xi}(\phi)e^{i(k\lambda-\omega t)}$ (where ξ~~ $q = \hat{q}(\phi)e^{i(k\lambda-\omega t)}$ (where q stands for any of the dependent variables u, v or Φ), with frequency and latitude dependent amplitudes corresponding to the initial wave. In this case, it is desirable to assess the accuracy of the zonal and meridional structures of the waves independently. A fast and simple way of doing so is using Hovmöller diagrams, where the temporal change in any direction is isolated by intersecting the fields along a fixed value of the other direction. This results in the following two diagrams:

(i) A ~~longitude-time~~ time-longitude diagram obtained by intersecting the fields at a certain latitude. The contour lines in the ~~longitude-time~~ time-longitude plane are the set of points satisfying $k\lambda - \omega t = const$ (for some real $const$). Thus, the expected pattern for this diagram is that of straight lines ~~whose slopes equal the~~ with slopes that equal the inverse of the wave's phase

speed k/ω. In order to avoid small fluctuations in the vicinity of latitudinal zero-crossings, we recommend using latitudinal intersects at or near local extrema.

(ii) A latitude-time diagram obtained by intersecting the fields at a certain longitude. For any two wave-fronts with equal phase $k(\lambda_2 - \lambda_1) = \omega(t_2 - t_1)$. Thus, holding λ fixed while varying t from t_1 to t_2 is equivalent to holding t fixed and varying λ from λ_1 to $\lambda_2 = \lambda_1 + \omega/k(t_2 - t_1)$. The resulting pattern is similar to that of a latitude-longitude diagram, but provides ~~a testament~~ an estimate of the time evolution as opposed to a momentary snapshot.

~~For~~ Likewise, for zonally propagating waves it is also desirable to isolate the errors in the phase speed and spatial structure. As discussed in Shamir and Paldor (2016), the frequently used spherical l_2 error entangles the two, and is therefore of lesser use for assessing the accuracy of propagating wave simulations. Thus for a more quantitative assessment we suggest using ~~a combination of Fourier analyses in longitude and time and a Hermite analysis in latitude to determine the dominant wave-numbers and wave-frequencies, and the dominant wave-modes (which determine the dominant meridional structure) of the simulated solution , respectively.The amplitude of the most dominant wave-component in each case can be compared to the amplitude of the analytic solution at the corresponding intersect, and~~ the ~~difference between the two provides a quantitative error-measure. The Fourier analysis can be trivially found using readily available Fast-Fourier-Transform libraries. The Hermite analysis was found in~~ relative difference between the Root-Mean-Square of the analytic solution and the simulated solutions, i.e.

$$\frac{\sqrt{I[q^2]} - \sqrt{I[q_a^2]}}{\sqrt{I[q_a^2]}}, \tag{7}$$

where the quantities q and q_a (which can be vectors) correspond to the simulated and analytic solutions, respectively, and where

$$I[q] = \frac{1}{4\pi} \int_0^{2\pi} \int_{-\pi/2}^{\pi/2} q(\lambda, \phi) \cos\phi d\phi d\lambda, \tag{8}$$

Henceforth we refer to the quantity in (7) as the structure-error since, as opposed to the ~~present work using the procedure described in Appendix **??**.~~

~~In order to attain reasonable accuracy in terms of the spectral analysis~~l_2 error, it is ~~recommended to integrate the initial fields forward in time for at least 10 wave-periods, with a sampling frequency of about 10 samples per period. The proposed integration and sampling times (denoted by T_f and T_s) for each of the four simulations, along with the wave-period (denoted by T), are given in Table **??**.~~

~~T (days) T_f (days) T_s (hours)**Rossby,** $H = 30$ **m**: 18.5 200 48 **EIG,** $H = 30$ **m**: 1.9 20 4 **Rossby,** $H = 0.5$ **m**: 127.8 1300 312 **EIG,** $H = 0.5$ **m**: 5.7 60 12 The wave-period T, integration time T_f, and sampling spacing T_s. Note, T is derived from the chosen test wave-parameters and is a characteristic of the waves, whereas T_f and T_s where chosen to attain reasonable accuracy in terms of the spectral analysis.~~ unaffected by phase speed errors (i.e. phase shifts in λ).

4 ~~Demonstration~~Results

~~In order to~~ In this section we demonstrate the usefulness of the Matsuno test case ~~we run~~ by applying the proposed procedure ~~using a simple~~ to both an equatorial channel finite-difference ~~shallow water model .~~ model and a global-scale spectral one. We then examine the stability of the selected waves/modes in a similar fashion to that used in Thuburn and Li (2000) for the wave-number 4 Rossby-Haurwitz wave. Finally, we demonstrate the possibility of using the analytic solutions obtained by Matsuno as a resolution convergence test.

4.1 Demonstration using an equatorial channel finite-difference model

The model is a spherical version of the Cartesian model used in ~~Gildor et al. (2016)~~Gildor et al. (2016), in which the integration forward in time is carried out using the ~~transport~~ conservation form of the SWEs

$$\frac{\partial U}{\partial t}+\frac{1}{a\cos\phi}\frac{\partial}{\partial\lambda}\left(\frac{U^2}{h}\right)+\frac{1}{a}\frac{\partial}{\partial\phi}\left(\frac{UV}{h}\right)-\frac{2UV\tan\phi}{ah}-2\Omega\sin\phi V=-\frac{g}{2a\cos\phi}\frac{\partial h^2}{\partial\lambda} \tag{9a}$$

$$\frac{\partial V}{\partial t}+\frac{1}{a\cos\phi}\frac{\partial}{\partial\lambda}\left(\frac{UV}{h}\right)+\frac{1}{a}\frac{\partial}{\partial\phi}\left(\frac{V^2}{h}\right)-\frac{(U^2-V^2)\tan\phi}{ah}+2\Omega\sin\phi U=-\frac{g}{2a}\frac{\partial h^2}{\partial\phi} \tag{9b}$$

$$\frac{\partial h}{\partial t}+\frac{1}{a\cos\phi}\left[\frac{\partial U}{\partial\lambda}+\frac{\partial(V\cos\phi)}{\partial\phi}\right]=0, \tag{9c}$$

where $U=hu$, $V=hv$ and h is the total layer thickness. The numerical scheme employs a standard finite difference shallow-water solver in which the time-differencing follows a leapfrog scheme (centre differencing in both time and space). The computations were done on an Arakawa C-grid. The ~~original Matlab code used in the following simulations is available as part of the on-line supporting material.~~

~~The model 's application was validated using both atmospheric and oceanic settings, i.e. using both $H=30$ m and $H=0.5$ m, totaling in four different initial waves (a Rossby wave and an EIG one for each value of H). The initial u,v,Φ fields of the Rossby (top row) and EIG (bottom row) waves obtained using the analytic expressions of Section 2 and the parameters of Section 3.1 are shown in Figure 1 for $H=0.5$ m. The corresponding fields for $H=30$ m differ only by e-folding latitude which is 11°, instead of 4°. Note that under the normalization~~ model contains provisions for a temporal Robert-Asselin filter, but the filter's coefficient was set to zero in the simulations of the present ~~paper the initial v field is independent of the wave type and is therefore identical on both rows, panels (b) and (e).~~

~~In all four cases, the computational domain was~~ section. In addition, the model includes no diffusion/viscosity terms.

The computational domain is $-180°\le\lambda\le180°$ and $-30°\le\phi\le30°$. The boundary conditions ~~were~~ are periodicity at the zonal boundaries $\lambda=\pm180°$ and vanishing meridional velocity at the channel's boundaries $\phi=\pm30°$. For ~~$H=30$ m,~~ the chosen wave-parameters the amplitude of the meridional velocity ~~at $\phi=\pm30°$ decays to $4e-03$ of its maximal value, and for $H=0.5$ m it decays to $2e-24$~~ $\hat{v}$ in (6) has an e-folding latitude of 11°, and its amplitude at $\phi=\pm30°$ decays to $4e-03$ of its maximal value, so ~~in both cases~~ the velocity outside the computational domain can be comfortably neglected. The grid-spacing

and time step ~~were~~ are $\Delta\lambda = \Delta\phi = 0.5^\circ$ and $\Delta t = 600$ seconds, which were found to yield stable solutions for at least ~~10~~ 100 wave-periods.

~~The resulting~~ Figure 1 shows the initial (top row) u, v, Φ, ξ, δ fields (where ξ and δ are the relative vorticity and divergence, respectively) of the chosen Rossby wave mode, and the resulting latitude-time (middle row) and time-longitude (bottom row) Hovmöller diagrams of the simulated ~~solutions for each of the initial waves are shown in Figure 2. In all cases, the latitude-time diagrams were obtained by intersecting v at $\lambda = -18^\circ$ (also indicated by vertical dashed white lines in Figure 1). The longitude-time diagrams were obtained by intersecting v at $\phi = 9^\circ$ for $H = 30$ m, and $\phi = 4^\circ$ for $H = 0.5$ m (the latter case is indicated by horizontal dashed white lines in Figure 1). Similar results are obtained using u or Φ, provided the meridional intersects are taken in the vicinity of their local extrema~~solution. The initial fields were obtained using the analytic expressions of Section 2 and wave-parameters of Section 3.1. The chosen intersects used in the calculation of the Hovmöller diagrams are indicated by white dashed lines superimposed on the initial fields, and are also provided in the Figure's caption. For the sake of legibility the shown time domain in each panel is ~~$9T \leq t \leq 10T$~~only the last wave periods of the simulation, i.e. $99T \leq t \leq 100T$, where T is the ~~corresponding~~ wave-period~~provided in Table **??**. Note that the~~. The fields are normalized on their global maximum at $t = 0$. Thus, white regions correspond to times at which the simulated solution exceeds the initial wave-amplitude, momentarily. With this in mind, recall that the patterns in the latitude-time diagrams are similar to ~~that~~ those of a latitude-longitude diagram~~and can, therefore ,~~, and can therefore be used to compare with the initial fields. In ~~all cases~~ general, the initial wave-structure is ~~clearly discernible after 10 wave-periods~~ preserved and the dominant slope in the time-longitude diagrams corresponds to the analytic slope indicated with dashed white lines ~~.~~

(bottom row). There are, however, some noticeable deviations: A slight east-west tilt can be observed in the latitude-time diagrams (middle row), but most egregiously, the divergence field is less regular than the other four. We return to this last point at the end of Section 4.3. The patterns in the latitude-time diagrams of the meridional velocity shown in panel (g) is precisely the expected pattern considering the westward propagation of the Rossby mode at $\lambda = -18^\circ$ in one wave-period after an integer number (99 in this case) of wave-periods.

Similarly, Figure 2 shows the initial (top row) u, v, Φ, ξ, δ fields of the chosen EIG wave mode, and the resulting latitude-time (middle row) and time-longitude (bottom row) Hovmöller diagrams of the simulated solution. Note that under the normalization used in the present paper the initial v field is independent of the wave type and is therefore identical in both figures. As in Figure 1 the dominant slope in the time-longitude diagrams (bottom row) agrees well with the analytic phase speed. In contrast to Figure 1 the latitude-time diagram in panel (g) appears to be $\pi/4$ out of phase (but can be any integer multiple of $\pi/4$) indicating that in this case there is a small (perhaps even tiny) phase speed error that accumulates over time. In addition, in contrast to the Rossby wave in Figure 1, the divergence field in this case is just as regular as the other four.

~~For a more quantitative assessment we use Fourier and Hermite analyses in order to locate the dominant wave-numbers, wave-modes, and wave-frequencies, and compare their amplitudes with the initial wave amplitudes. Figure 3 contains~~ The structure-error defined in (7) is shown in Figure 3 for both Rossby (top) and EIG (bottom) waves as a function of time. In both cases the structure-error fluctuates about a mean value of less than 1% and there is no visible trend throughout the simulation time of 100 wave-periods.

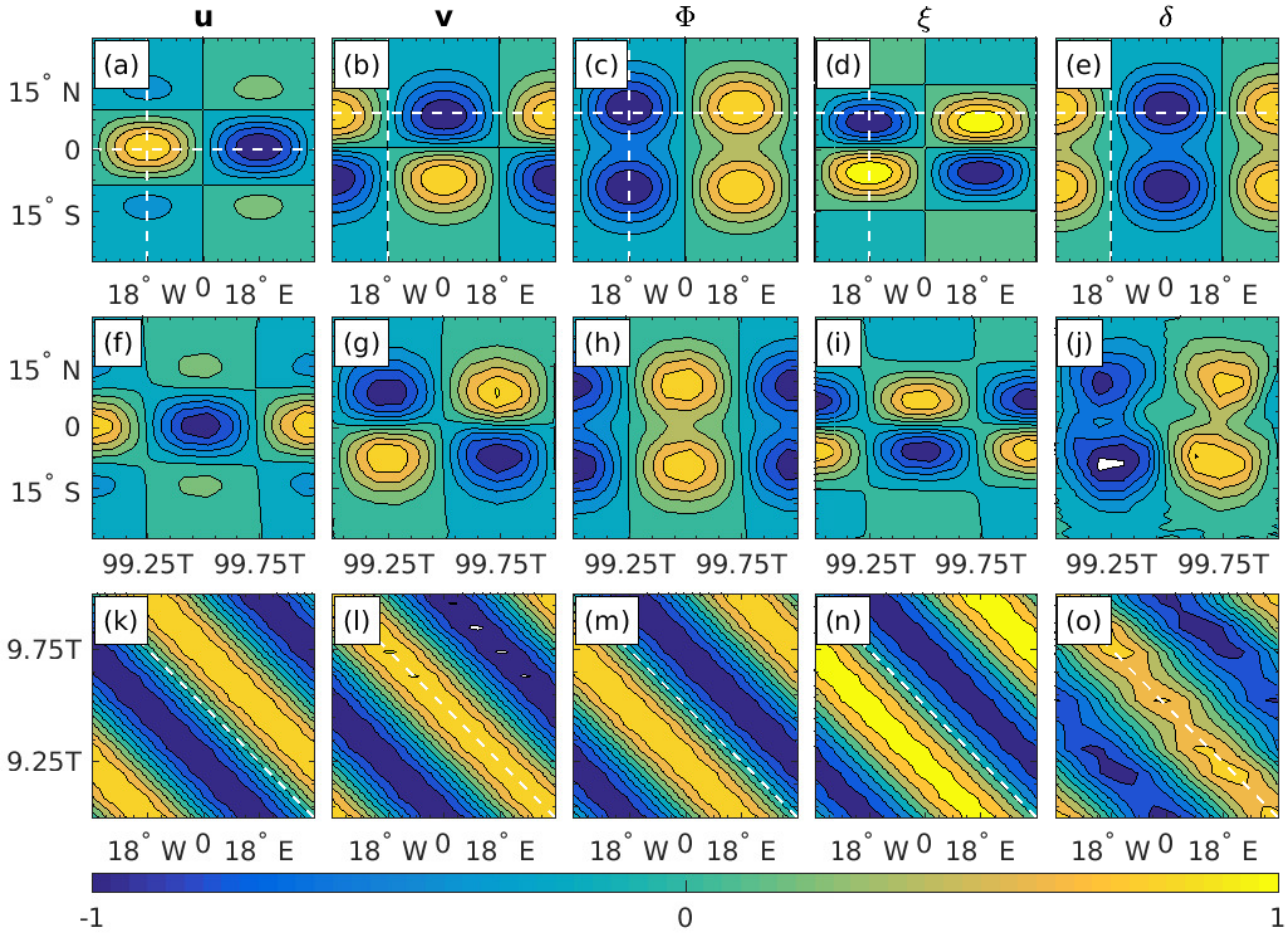

Figure 1. Top row: the initial u, v, Φ, ξ, δ Rossby wave fields (top row), obtained using the analytic expressions of Section 2 and wave-parameters of Section 3.1. Middle row: latitude-time Hovmöller diagrams~~of the simulated solutions. (a)–(d) Latitude-time diagrams~~, obtained by intersecting ~~v~~ the fields at $\lambda = -18°$ ~~.~~(~~e~~) –(~~h~~also indicated by white vertical dashes lines in the top row)~~Longitude-time~~. Bottom row: longitude-time Hovmöller diagrams, obtained by intersecting ~~v~~ u at ~~$\phi = 9°$ for $H = 30$ m,~~ $\phi = 0°$ and ~~$\phi = 4°$ for $H = 0.5$ m~~ all other fields at $\phi = 9°$ (~~the later case is~~ also indicated by ~~horizontal dashed~~ white horizontal dashes lines in ~~Figure 1). For the sake of legibility the shown time domain in each panel is $9T \leq t \leq 10T$, where T is~~ the ~~corresponding wave-period provided in Table **??**. For comparison, the analytic (initial) slope in each case is indicated using dashed white line (bottom~~ top row). The ~~amplitude in each panel is~~ fields are normalized on ~~the~~ their global maximum at $t = 0$~~, i.e. $v / \max_{\lambda,\phi} |v(t = 0)|$, which is~~ The wave-period for the ~~same in all cases~~chosen wave-parameters is $T = 18.5$ days. Contour-levels range from -1.0 to $+1.0$ by 0.2.

4.2 Demonstration using a global-scale spectral model

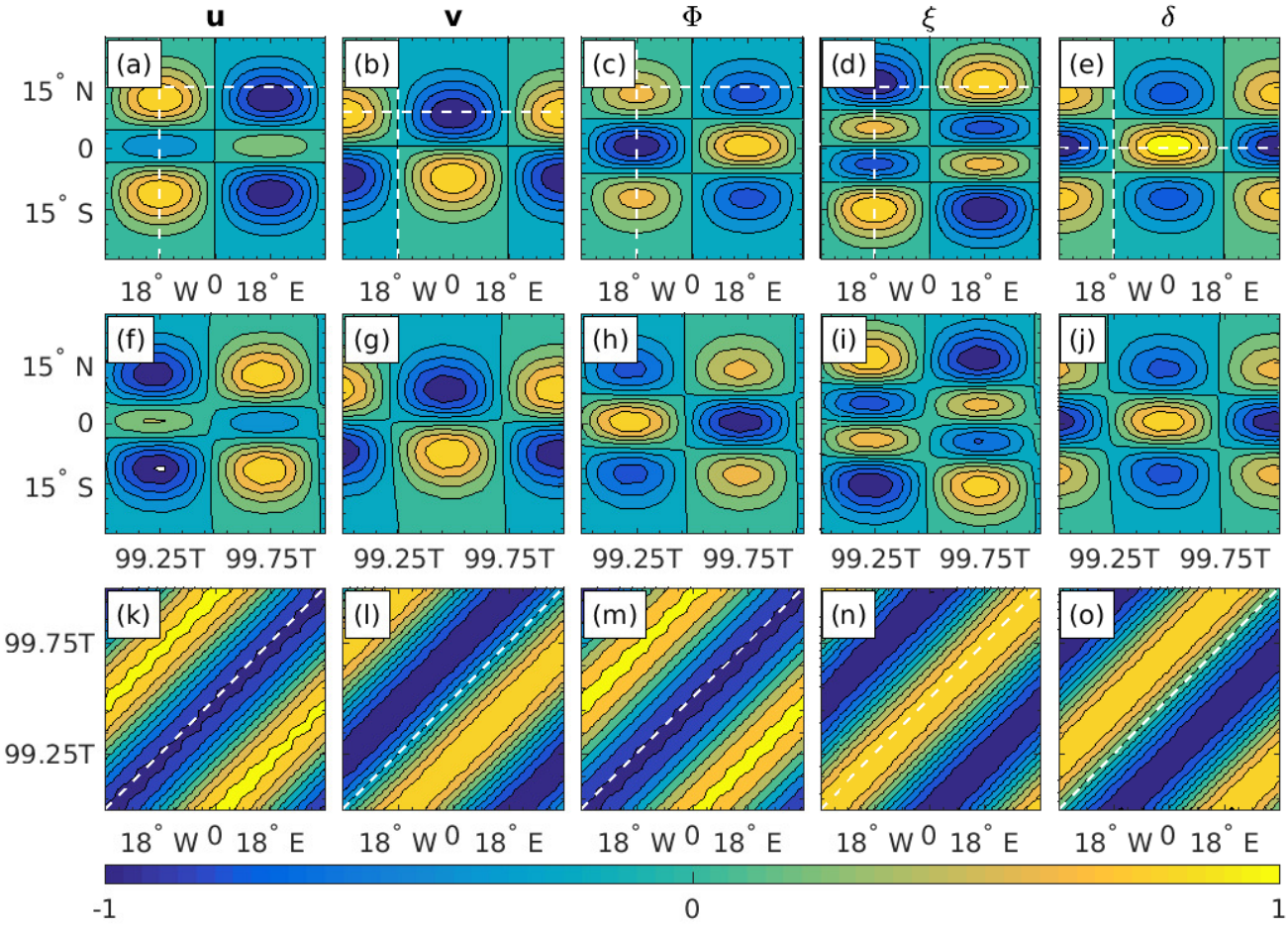

Figure 2. Top row: the initial u, v, Φ, ξ, δ EIG wave fields (top row), obtained using the analytic expressions of Section 2 and wave-parameters of Section 3.1. Middle row: latitude-time Hovmöller diagrams, obtained by intersecting the fields at $\lambda = -18^\circ$ (also indicated by white vertical dashes lines in the top row). Bottom row: longitude-time Hovmöller diagrams, obtained by intersecting v at $\phi = 9^\circ$, δ at $\phi = 0^\circ$ and all other fields at $\phi = 15^\circ$ (also indicated by white horizontal dashes lines in the top row). The fields are normalized on their global maximum at $t = 0$. The wave-period for the chosen wave-parameters is $T = 1.9$ days. Contour-levels range from -1.0 to $+1.0$ by 0.2.

To demonstrate the applicability of the Matsuno wave as a test case for global-scale model we use the Geophysical Fluid Dynamics Laboratory's (GFDL's) spectral transformed shallow water model which uses the Spherical Harmonics as its basis functions. The chosen spectral resolution was T85, i.e. a triangular truncation where the highest wave-number and total wave-number retained both equal 85. The chosen time step was $\Delta t = 600$ seconds, as in the equatorial channel model. The model contains provisions for hyper-diffusion terms as well as a temporal Robert-Asselin filter, but the coefficients of both were set to zero for the simulations described below.

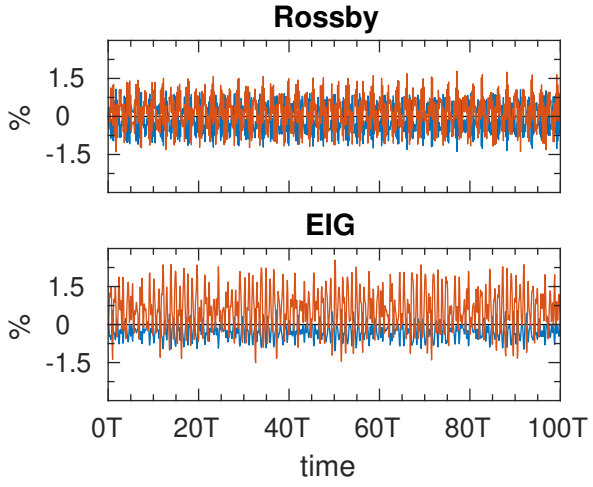

Figure 3. The structure-error defined in (7) is shown in Figure 3 for both the Rossby (top) and EIG (bottom) waves as a function of time. Blue: calculated for the velocity vector $\sqrt{u^2+v^2}$. Red: calculated for the geopotential Φ.

Figures 4 and 5 show simulations of the same initial Rossby and EIG waves as in Figures 1 and 2, and the resulting power-spectra of the simulated solutions obtained using the same latitudinal and longitudinal intersects used for the latitude-time (middle row) and time-longitude (bottom row) Hovmöller diagrams in Figure 2, and $t = 10T$ as the time intersect, where T in each case is the corresponding of the simulated solution, obtained using GFDL's global-scale spectral model. Note, that unlike Figures 1 and 2, the top row corresponds to the simulated solutions at $t = 4$ hours, and not the initial fields at $t = 0$.

Unlike the the equatorial channel model, the simulated divergence field of the initial Rossby wave in Figure 4 remains as regular as the four other fields. The structure in the latitude-time diagrams (middle row) are at slightly out of phase after 99 wave-periods. The simulated EIG wave in Figure 5 is at least $\pi/4$ out of phase after 99 wave-periods. Finally, structure-error in Figure 6 is generally similar to the simulations of the equatorial channel model, it fluctuates about a mean value of less than 1% and there are no visible trends throughout the 100 wave-period listed in Table **??**. In all cases the dominant wave-number and wave-mode clearly match the initial values $k = 5$ and $n = 1$. Likewise the dominant frequencies match the initial ones indicated on the figure using black dashed linessimulations. Recall that the structure-error defined in (7) is insensitive to phase differences.

The first and second most dominant wave components of the simulated solutions are summarized in Table **??**, compared to the wave components of the analytic (initial) solutions. The errors in the frequencies were derived from the spectral resolution, which for (about) 10 wave-periods integration is (about)10% of the initial wave's frequency

4.3 Smoothness and stability

In this section we examine the generation of small-scale features and the stability of the proposed wave solutions in a similar fashion to that used in Thuburn and Li (2000) for the original Rossby-Haurwitz wave-number 4.

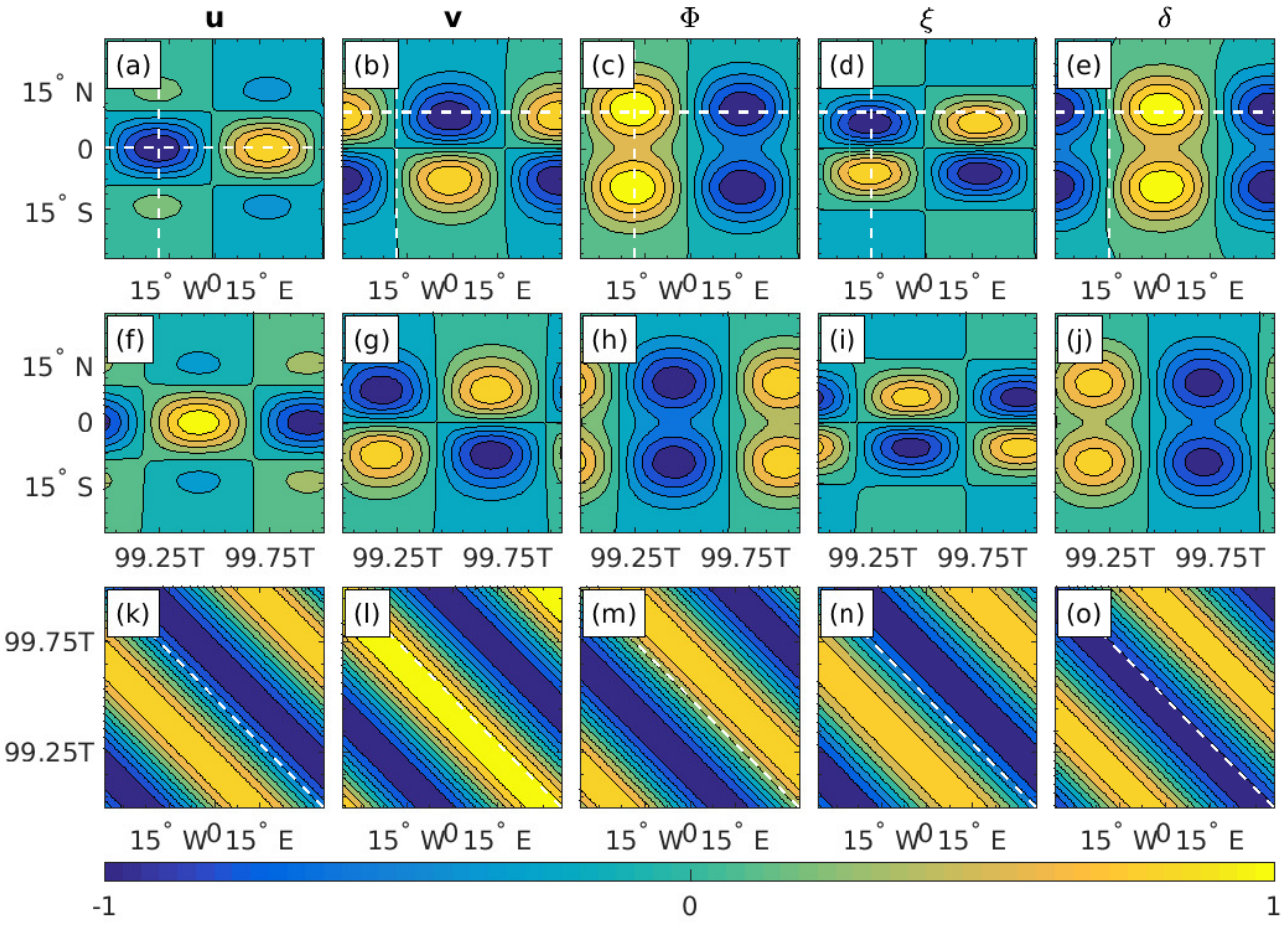

Figure 4. ~~Power-spectra of the simulated solutions. Left column: Power-spectra in k-space obtained using Fourier analyses of longitudinal series at $(\phi,t)=(9°,10T)$ and $(\phi,t)=(4°,10T)$ for $H=30$ m and $H=0.5$ m, respectively~~Same as Figure 1, ~~where T in each case is the corresponding wave-period provided in Table **??**. Middle column: Power-spectra in n-space obtained using Hermite analyses of latitudinal series at $(\lambda,t)=(-18°,10T)$. Right column: Power-spectra in ω-space obtained~~ but using ~~Fourier analyses of time series at $(\lambda,\phi)=(-18°,9°)$ and $(\lambda,\phi)=(-18°,4°)$ for $H=30$ m and $H=0.5$ m, respectively~~GFDL's global-scale spectral model. ~~Since the fields are real, only a one-sided power spectrum is shown~~Note, ~~i.e. for $|\omega|$. In order to facilitate the comparison~~unlike Figure 1, the ~~initial frequencies for the chosen parameters in Section 3.1 are also indicated in the figure using black dashed lines. For~~ top row corresponds to the ~~sake of presentation all power spectra are multiplied by 10^{-8}~~simulated solutions at $t=4$ hours.

In Thuburn and Li (2000), the generation of small-scale features and the potential enstrophy cascade is observed by examining the potential vorticity field, which generates tongues that warp up around themselves and break the initial east-west symmetry. For the small wave-amplitude $A=10^{-5}$ m s^{-1} used in the present work, the potential vorticity is dominated by the planetary

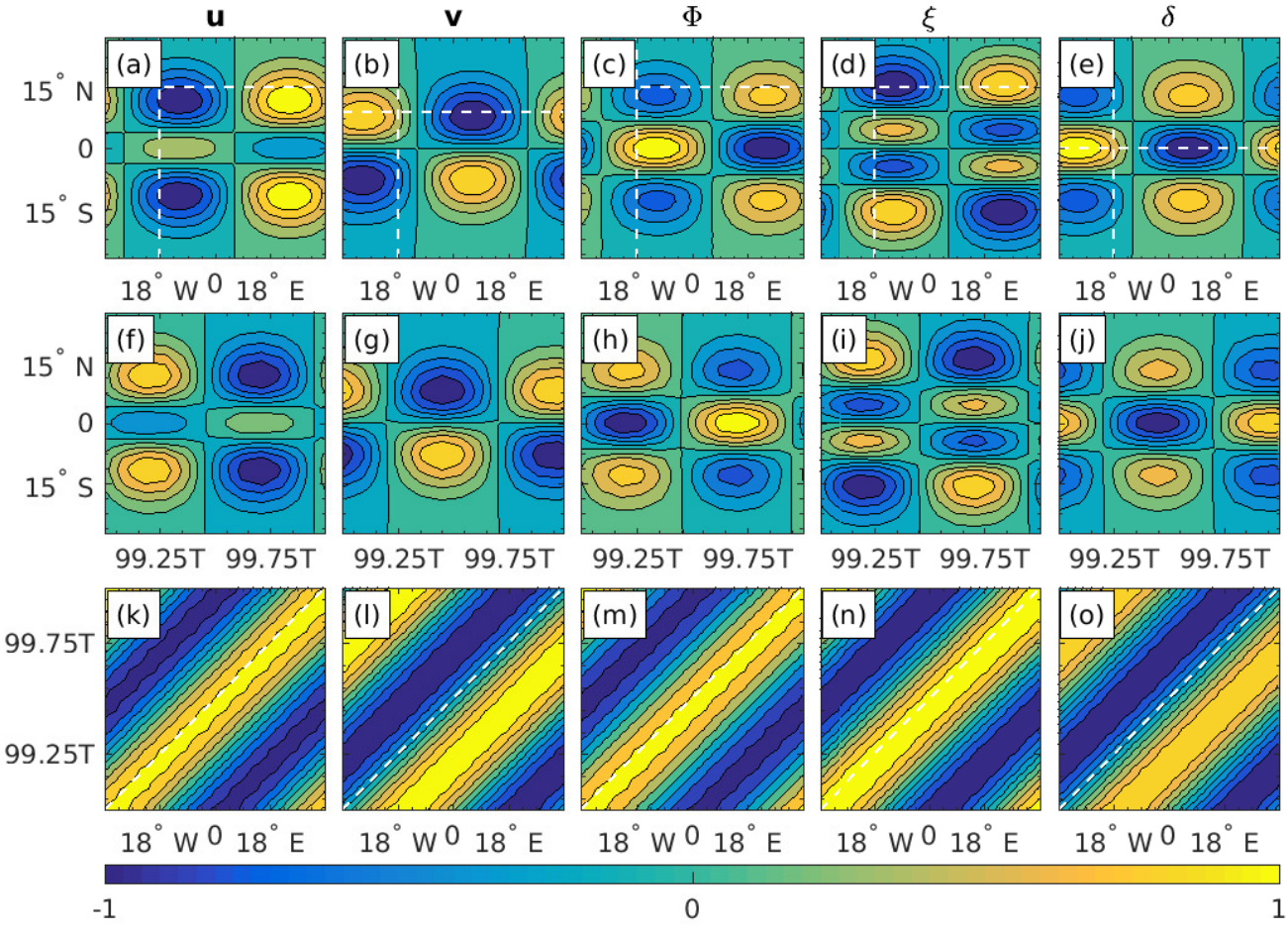

Figure 5. Same as Figure 2, but using GFDL's global-scale spectral model. Note, unlike Figure 2, the top row corresponds to the simulated solutions at $t = 4$ hours.

vorticity which is 5-6 orders of magnitudes (depending on the wave) larger than the relative vorticity. Thus, instead of the potential vorticity we examine the relative vorticity (as well as the geopotential). Figures 1-2, as well as Figures 4-5, show the evolution of these two fields between $t = 99T$ and $t = 100T$, where T is the wave-period in each case. ~~The errors in the amplitudes of the first most dominant wave components were estimated using the amplitudes of the second most dominant ones, and the errors in the amplitudes of the second most dominant wave components were estimated using the amplitudes of the third most dominant ones.~~

Clearly, both fields remain regular throughout the simulations and do not develop small-scale features like the ones observed in Thuburn and Li (2000). Recall that the simulations in the present work were carried out without any diffusion/viscosity

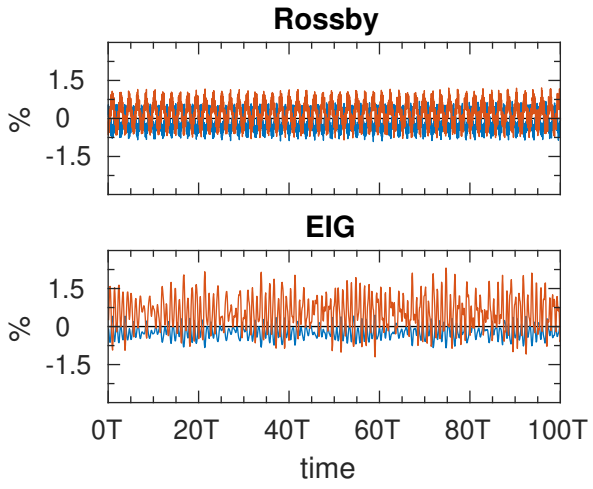

Figure 6. Same as Figure 3, but using GFDL's global-scale spectral model.

terms. Thus, the simulations remain stable for at least 100 wave-periods with no need to remove potential enstrophy at the grid scale.

~~k $|\hat{F}_k|$ (m sec^{-1}) n $|\hat{F}_n|$ (m sec^{-1}) $|\omega|$ (rad day^{-1}) $|\hat{F}_\omega|$ (m sec^{-1}) **Rossby,** $H = 30$ **m**: Analytic 5 6.29e-09 1 2.39e-09 3.40e-01 6.29e-09 1st most dominant 5 6.39e-09 ± 9.99e-15 1 3.68e-09 ± 4.46e-10 3.42e-01 ± 3.11e-02 6.32e-09 ± 4.90e-10 2nd most dominant 35 9.99e-15 ± 8.86e-15 0 4.46e-10 ± 2.19e-10 3.11e-01 ± 3.11e-02 4.90e-10 ± 4.44e-10 **EIG,** $H = 30$ **m**: Analytic 5 6.29e-09 1 2.83e-09 3.34e+00 6.29e-09 1st most dominant 5 6.06e-09 ± 4.53e-15 1 5.81e-09 ± 1.82e-10 3.43e+00 ± 3.12e-01 5.61e-09 ± 1.88e-09 2nd most dominant 10 4.53e-15 ± 3.95e-15 2 1.82e-10 ± 1.14e-10 3.12e+00 ± 3.12e-01 1.88e-09 ± 1.10e-09 **Rossby,** $H = 0.5$ **m**: Analytic 5 5.46e-09 1 1.17e-09 4.92e-02 5.46e-09 1st most dominant 5 5.62e-09 ± 3.27e-15 1 5.30e-09 ± 9.82e-10 4.79e-02 ± 4.79e-03 5.11e-09 ± 1.37e-09 2nd most dominant 52 3.27e-15 ± 2.87e-15 2 9.82e-10 ± 1.80e-10 5.26e-02 ± 4.79e-03 1.37e-09 ± 1.02e-09 **EIG,** $H = 0.5$ **m**: Analytic 5 5.46e-09 1 4.57e-09 1.10e+00 5.46e-09 1st most dominant 5 5.43e-09 ± 1.25e-15 1 5.58e-09 ± 2.27e-10 1.14e+00 ± 1.04e-01 3.76e-09 ± 3.11e-09 2nd most dominant 55 1.25e-15 ± 1.22e-15 2 2.27e-10 ± 2.21e-10 1.04e+00 ± 1.04e-01 3.11e-09 ± 1.16e-09 The first and second most dominant wave components of the simulated solutions, compared to the wave components of the analytic (initial) solutions. The dominant components were obtained from the same analyses as in Figure 3, i.e. using the same series. The frequencies errors were derived from the spectral resolution, which is about 10% for the ten wave-periods integration. The errors in the amplitudes of the first most dominant wave components were estimated using the amplitudes of the second most dominant component, and the errors in the amplitudes of the second most dominant wave components were estimated using the amplitudes of the third most dominant component. $|\hat{F}_k|$, $|\hat{F}_n|$ and $|\hat{F}_\omega|$ denote the amplitudes of the wave component in the k, n and ω spaces, respectively.~~ In order to examine the stability of the chosen initial waves we repeat the simulations of the previous section with an added perturbation (white noise) to the initial fields. We demonstrate the stability of the waves using only the global-scale model, which was found to yield more stable results when adding the perturbation.

~~The overall scenario that emerges from the spectral analyses is similar to that of the~~ Figures 7 and 8 show the perturbed Rossby and EIG waves, respectively, at $t = 4$ hours (top) and the resulting latitude-time (middle row) and time-longitude (bottom row) Hovmöller diagrams of the simulated solution, obtained using GFDL's global-scale spectral model. The initial perturbation in these figures consist of a uniformly distributed random white noise with amplitude of 5% of the field's amplitude added to each of the fields u,~~namely that the initial waves remain dominant after 10 wave-periods.~~ v,Φ. Specifically, let q stands for any of the variables u,v or Φ then the initial perturbation is given by

$$q = q_a + 0.05 \max_{\lambda,\phi} |q_a|(2R - 1), \tag{10}$$

where q_a is the analytic solutions obtained as in Section 2, and R is a uniformly sampled random matrix with elements in $(0, 1)$ whose dimensions are the same as q_a (in the present work a different R was drawn for each of the three variables).

Overall, the perturbed waves seem to be stable. The u,v and Φ fields are almost as regular as those of the non-perturbed waves, except for the zero-contour. The small-scale features in the vorticity field of the perturbed Rossby smooth out with time, in contrast to the potential vorticity field of the Rossby-Haurwitz wave-number 4. On the other hand, the perturbed Rossby wave divergence field is completely eroded. The vorticity and divergence fields of the perturbed EIG wave are not as regular as those of the non-perturbed wave. However, ~~it provides a quantitative measure of the errors in the simulated solutions, since for an ideal model the amplitudes of the first most dominant wave components should be the same as the analytic ones. Thus, the closer the amplitudes of the first~~ they do become smoother with time and the initial wave remains the most dominant wave ~~components to the analytic ones~~ throughout the entire 100 wave-period simulation. The structure-error in Figure 9 is similar to the previous ones in Figures 3 and 6. These results are quite surprising. We would expect a sufficiently large perturbation to excite other modes, regardless of the waves' stability.

Both the non-perturbed Rossby wave simulated using the equatorial channel model, and the ~~smaller the amplitudes of the second most dominant wave components, the better~~perturbed Rossby wave simulated using the global-scale mode indicate that the divergence field is more sensitive than the other four fields of the Rossby wave. An immediate suspect in this regard is the divergence field amplitude, which is small for the chosen Rossby wave. For reference the meridional wind amplitude for the chosen waves parameters (of both the Rossby and EIG waves) is $6.4e-6$, whereas the Rossby wave divergence field amplitude is $2.6e-12$. On the other hand, the divergence field amplitude is only one order of magnitude smaller than the vorticity field amplitude, which is $2.7e-11$. Regardless of the cause, the fact the all other four fields remain quite regular while the divergence field is completely eroded suggests that the small-but-significant divergence field described by Phillips (1959) is in fact a small-and-insignificant one.

4.4 Convergence test for the linear shallow water models

In addition to the test cases proposed by Williamson et al. (1992) a resolution convergence test of linearized SWEs in which the simulations are compared to higher order simulations is also useful for ensuring that the errors decrease with the increase in resolution. In this section we demonstrate that Matsuno's analytic wave solutions can be used for this purpose. We use the equatorial channel model which can be easily turned into a linear shallow water model.

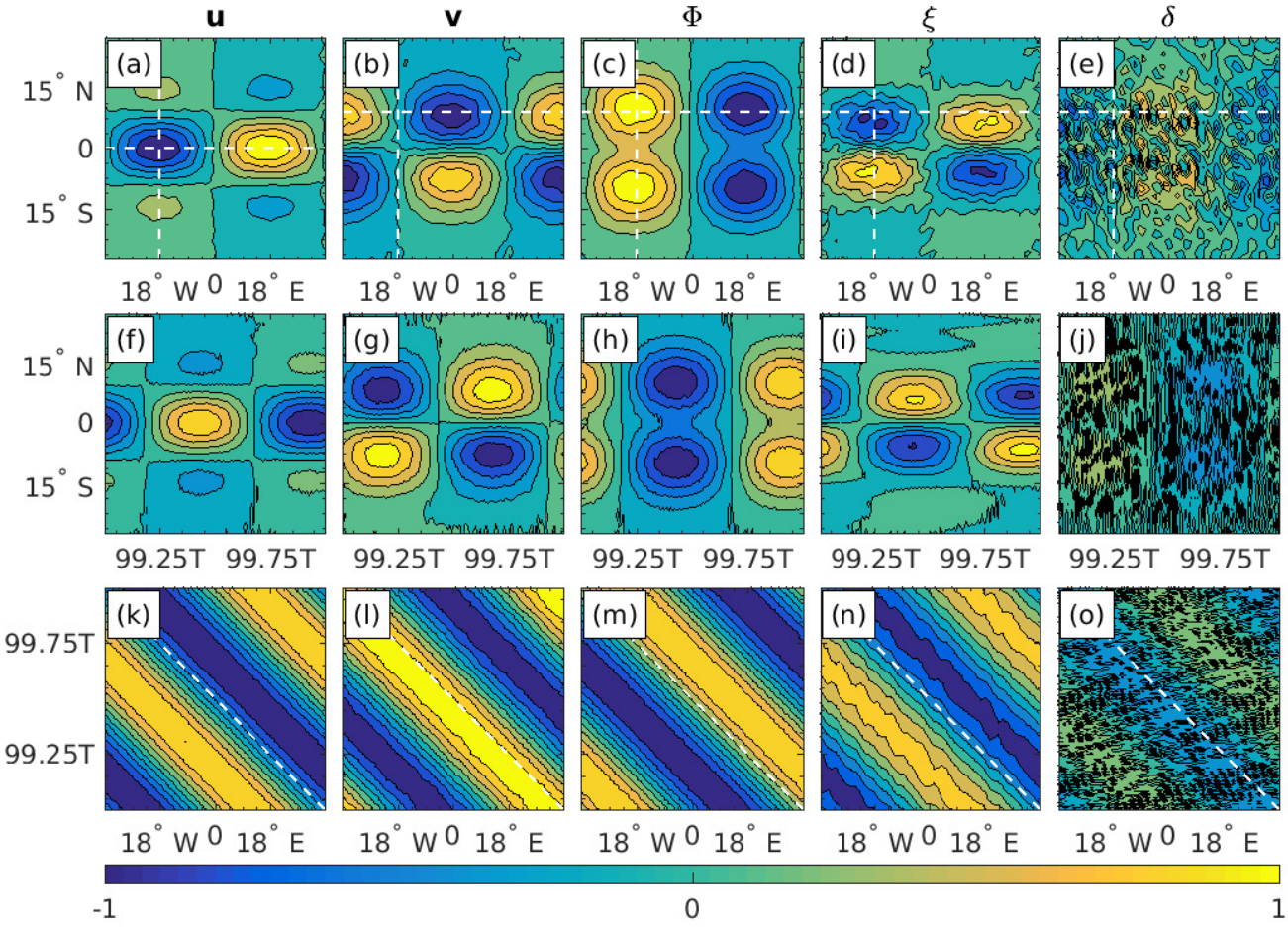

Figure 7. Same as Figure 4, but for the perturbed Rossby wave.

Figure 10 shows the structure-error in absolute value as a function of the grid-spacing $\Delta = \Delta\lambda = \Delta\phi$, from $\Delta = 2.5°$ to $\Delta = 0.5°$ every $0.25°$. For each resolution, the initial non-perturbed waves were integrated for 100 wave-periods. As an estimate of the structure-error at each resolution we use the time-series averages (indicated by dots). The error-bars were estimated using the standard deviations of the entire time-series. As the resolution increase from $\Delta = 2.5°$ to $\Delta = 0.5°$, the structure-error time-series average decrease from about about 2% to less than 1%, while the standard deviation decrease from about 2% to about 0.5%. The time step across all resolutions in this figure was held fixed at $\Delta t = 600$ seconds. Attempting to further increase the resolution while holding the time step fixed cause the equatorial channel model to blow up, so a smaller time step is required in order to further improve the accuracy.

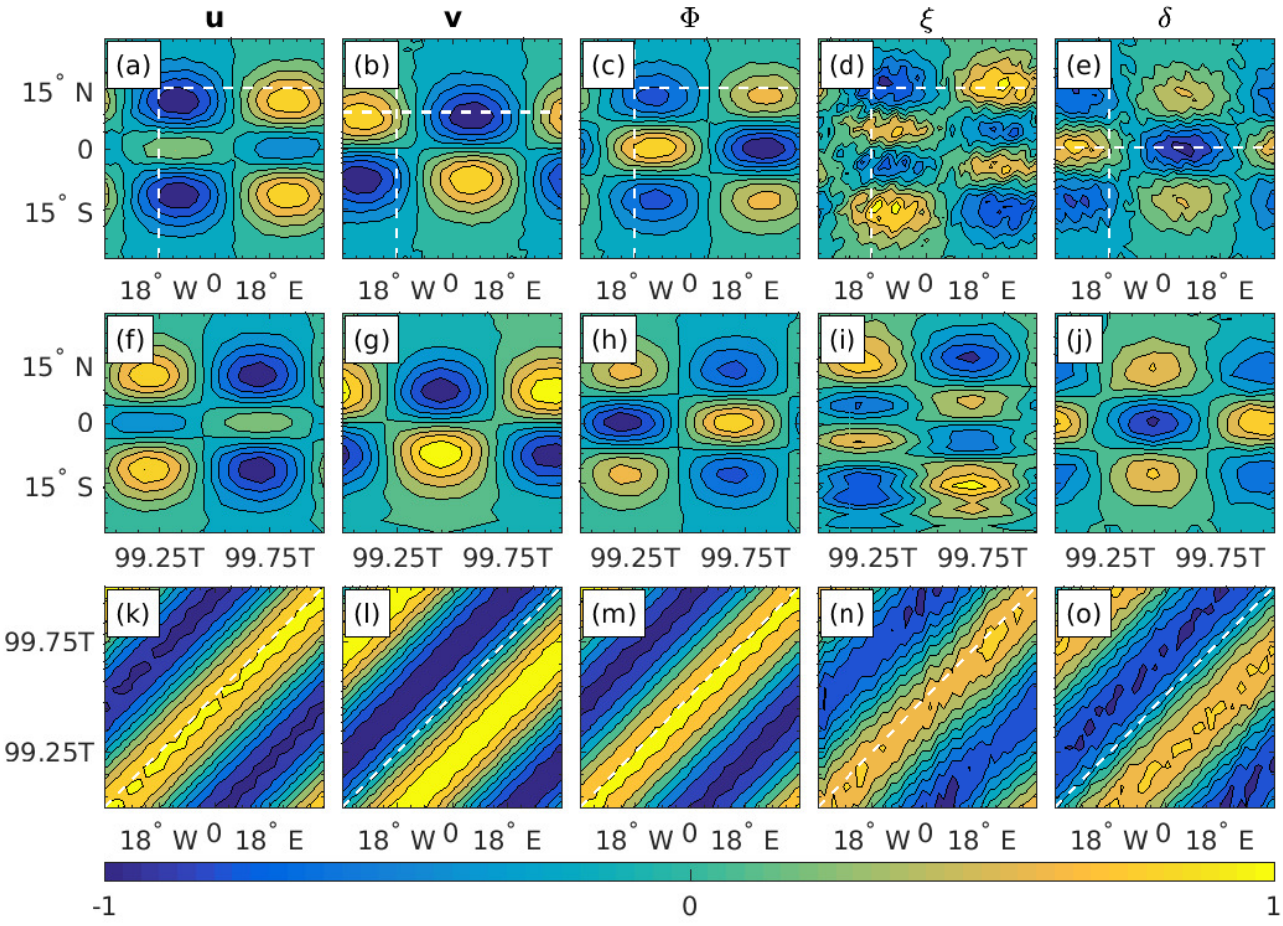

Figure 8. Same as Figure 5, but for the perturbed EIG wave.

5 Concluding remarks

As vertical resolutions in atmospheric and oceanic models increase it is essential to assess the accuracy with which they resolve baroclinic wave modes, typified by small gravity wave phase speed, in addition to the barotropic mode. To this end we propose to use a similar procedure to ~~the one~~ that used in the Rossby-Haurwitz test case but replace the initial conditions. Instead of using the analytic solutions obtained by ~~Haurwitz (1940)~~Haurwitz (1940), which are only accurate for large gravity wave speeds such as those of the barotropic mode, we propose to use the analytic solutions obtained by ~~Matsuno (1966)~~ Matsuno (1966), which are accurate for smaller gravity wave speeds such as those of the baroclinic modes.

~~Unlike the solutions obtained by Haurwitz (1940) for the non-divergent barotropic vorticity equation, the solutions of the SWEs obtained by Matsuno (1966) fully account for the velocity divergence. As a result an initial wave can be accurately~~

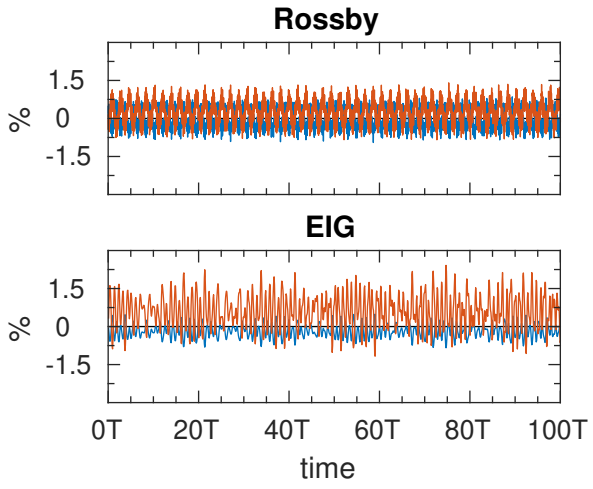

Figure 9. Same as Figure 6, but for the perturbed Rossby (top) and EIG (bottom) waves.

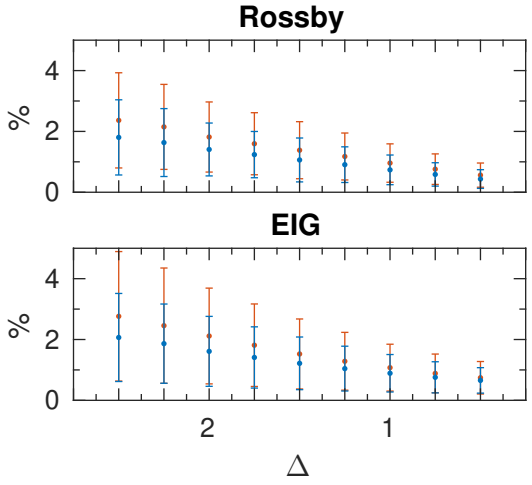

Figure 10. Structure-error in absolute value as a function of the grid-spacing $\Delta = \Delta\lambda = \Delta\phi$, from $\Delta = 2.5^\circ$ to $\Delta = 0.5^\circ$ every 0.25°. The points correspond to the time averaged structure-error over 100 wave-periods, and the error-bars are determined from the standard deviation. Blue: calculated for the velocity vector $\sqrt{u^2 + v^2}$. Red: calculated for the geopotential Φ

~~simulated for long times and the simulated solution can be compared to the analytic solution to obtain a quantitative assessment.~~ While Matsuno's solutions apply for the equatorial β-plane, they approximate the solutions of the SWEs on the sphere for the speeds of gravity waves found in the baroclinic modes in the atmosphere~~and oceans~~, and as demonstrated in the present work can be accurately simulated in ~~spherical coordinate models . Finally, in contrast to the barotropic mode, the baroclinic modes are confined to narrow equatorial band. Therefore, the proposed test can also be used to test tropical models~~both equatorial channel and global-scale models in spherical coordinates. In addition, unlike the original Rossby-Haurwitz wave-number 4,

the chosen initial waves of the present test case remain stable for at least 100 wave-periods, which for the chosen Rossby wave correspond to about 1850 days.

While the solutions of the SWEs obtained by Matsuno (1966) account for the small divergence field missing from the non-divergent Rossby-Haurwitz waves, the results of the present study suggest that this missing divergence field is insignificant.

Ideally, we expect the proposed test case to stand on an equal footing alongside the Rossby-Haurwitz one, but in the words of ~~Williamson et al. (1992)~~Williamson et al. (1992): "The test will only become standard to the extent that the community finds it useful".

Code availability. For the sake of re-producibility, the following files are available online as part of the supplementary material of this work:

matsuno.m: A Matlab code for computing the analytic solutions obtained by Matsuno as described in section 2. The code can be used to evaluate the horizontal velocity fields u and v, in m s^{-1}, and the geopotential field Φ, in m^2 s^{-2} (or h in m) for all $t \geq 0$.

shallow_water_model.m: A Matalb code containing the shallow water model used in section 4.1.

6 ~~The roots of the cubic equation~~

~~For any combination of wave-number and wave-mode, k and n, the wave-frequencies are given by the three roots of the cubic equation in . These roots can be written in a closed analytic form using the general solution of the cubic equation (e.g. Abramowitz and Stegun, 1964):~~

$$\omega_{n,k,j} = -\frac{1}{3}\left(\Delta_j + \frac{\Delta_0}{\Delta_j}\right), \quad \text{for} \quad j = 1,2,3$$

~~where j stands for the three roots, and where~~

$$\Delta_0 = 3\left[gHk^2 + \frac{2\Omega\sqrt{gH}}{a}(2n+1)\right],$$

$$\Delta_j = \left[\frac{\Delta_4 + \sqrt{\Delta_4^2 - 4\Delta_0^3}}{2}\right]^{1/3} \times \exp\left(\frac{2\pi j}{3} i\right),$$

$$\Delta_4 = -\frac{54\Omega g H k}{a}.$$

Data availability. TEXT

~~Given the definitions in , the explicit expressions for the frequencies of the Rossby, WIG and EIG waves are obtained by sorting the values in as follows:~~

Code and data availability. TEXT

Sample availability. TEXT

6 ~~The Hermite transform~~

~~Let $\xi(\phi)$ denote a latitudinal series (i.e. an intersect along specific longitude and time) of any one of the dependent variables. We seek approximate series expansion of the form~~

$$\xi(\phi) = \sum_{n=0}^{N} \hat{\xi}_n \hat{H}_n \left[\epsilon^{1/4}\phi\right] \exp\left[-\frac{1}{2}\epsilon^{1/2}\phi^2\right],$$

~~where $\hat{\xi}_n$ are spectral coefficients, ϵ is Lamb's parameter defined in the text, and $\hat{H}_n$ are the normalized Hermite polynomials of degree n. The normalization of the Hermite polynomials implies that they are orthonormal on $[-\infty,\infty]$ with respect to the weight function $\exp(-x^2)$, i.e.~~

$$\int_{-\infty}^{\infty} \hat{H}_n(x)\hat{H}_m(x)e^{-x^2}\,dx = \begin{cases} 1 & \text{for } n = m \\ 0 & \text{for } n \neq m. \end{cases}$$

~~It follows that the spectral coefficients are given by~~

$$\hat{\xi}_n = \int_{-\infty}^{\infty} \xi(\phi)\hat{H}_n \left[\epsilon^{1/4}\phi\right] \exp\left[-\frac{1}{2}\epsilon^{1/2}\phi^2\right] d(\epsilon^{1/4}\phi).$$

~~In order to apply the Hermite analysis on the finite meridional domain we assume that $\xi(\phi)$ decays sufficiently fast so that it can be approximated by zero outside the computational domain, $[-\pi/6,\pi/6]$ in the present work (or $[-\pi/2,\pi/2]$ for global-scale models). In particular, in the present work we assume that the following approximation holds~~

$$\int_{-\pi/6}^{\pi/6} \xi(\phi)\hat{H}_n \left[\epsilon^{1/4}\phi\right] \exp\left[-\frac{1}{2}\epsilon^{1/2}\phi^2\right] d(\epsilon^{1/4}\phi) \approx$$

$$\int_{-\infty}^{\infty} \xi(\phi)\hat{H}_n \left[\epsilon^{1/4}\phi\right] \exp\left[-\frac{1}{2}\epsilon^{1/2}\phi^2\right] d(\epsilon^{1/4}\phi).$$

~~Finally, the integral in was evaluated using the trapezoidal rule.~~

Author contributions. NP conceived the idea of standardizing the Matsuno test case for General Circulation Models in spherical coordinates. IY adopted the Cartesian shallow water model used in Gildor et al. (2016) to spherical coordinates and was responsible for the numerical simulations. OS analyzed the numerical results, prepared the manuscript and ran the GFDL spectral global model.

Competing interests. The authors declare that they have no conflict of interest.

Disclaimer. TEXT

Acknowledgements. H-Z. Krugliak and Dr. C. I. Garfinkel of HU helped us install and run the GFDL model. We also acknowledge the helpful discussions we had with Dr. Y. De-Leon of HU.

References

Abramowitz, M. and Stegun, I. A.: Handbook of Mathematical Functions with Formulas, Graphs, and Mathematical Tables, vol. 56 of *National Bureau of Standards Applied Mathematics Series*, Dover, https://doi.org/10.1119/1.15378, 1964.

Bosler, P., Wang, L., Jablonowski, C., and Krasny, R.: A Lagrangian particle/panel method for the barotropic vorticity equations on a rotating sphere, Fluid Dynamics Research, 46, 031 406, 2014.

Chelton, D. B., Deszoeke, R. A., Schlax, M. G., El Naggar, K., and Siwertz, N.: Geographical variability of the first baroclinic Rossby radius of deformation, Journal of Physical Oceanography, 28, 433–460, 1998.

De-Leon, Y. and Paldor, N.: Zonally propagating wave solutions of Laplace Tidal Equations in a baroclinic ocean of an aqua-planet, Tellus A, 63, 348–353, https://doi.org/10.1111/j.1600-0870.2010.00490.x, 2011.

Garfinkel, C. I., Fouxon, I., Shamir, O., and Paldor, N.: Classification of eastward propagating waves on the spherical Earth, Quarterly Journal of the Royal Meteorological Society, 143, 1554–1564, 2017.

Gildor, H., Paldor, N., and Ben-Shushan, S.: Numerical simulation of harmonic, and trapped, Rossby waves in a channel on the midlatitude β-plane, Quarterly Journal of the Royal Meteorological Society, 142, 2292–2299, 2016.

Haurwitz, B.: The motions of the atmospheric disturbances on the spherical earth, J. mar. Res, pp. 254–267, 1940.

Hoskins, B. J.: Stability of the Rossby-Haurwitz wave, Quarterly Journal of the Royal Meteorological Society, 99, 723–745, https://doi.org/10.1002/qj.49709942213, https://rmets.onlinelibrary.wiley.com/doi/abs/10.1002/qj.49709942213, 1973.

Jablonowski, C.: Adaptive grids in weather and climate modeling, Ph.D. thesis, University of Michigan, Ann Arbor, MI, USA, 2004.

Jablonowski, C. and Williamson, D. L.: A baroclinic instability test case for atmospheric model dynamical cores, Quarterly Journal of the Royal Meteorological Society, 132, 2943–2975, 2006.

Jablonowski, C., Oehmke, R. C., and Stout, Q. F.: Block-structured adaptive meshes and reduced grids for atmospheric general circulation models, Philosophical Transactions of the Royal Society of London A: Mathematical, Physical and Engineering Sciences, 367, 4497–4522, 2009.

Lauritzen, P. H., Jablonowski, C., Taylor, M. A., and Nair, R. D.: Rotated versions of the Jablonowski steady-state and baroclinic wave test cases: A dynamical core intercomparison, Journal of Advances in Modeling Earth Systems, 2, 2010.

Li, X., Peng, X., and Li, X.: An improved dynamic core for a non-hydrostatic model system on the Yin-Yang grid, Advances in Atmospheric Sciences, 32, 648–658, 2015.

Matsuno, T.: Quasi-geostrophic motions in the equatorial area, Journal of the Meteorological Society of Japan. Ser. II, 44, 25–43, 1966.

Mohammadian, A. and Marshall, J.: A "vortex in cell" model for quasi-geostrophic, shallow water dynamics on the sphere, Ocean Modelling, 32, 132–142, 2010.

Paldor, N., De-Leon, Y., and Shamir, O.: Planetary (Rossby) waves and inertia–gravity (Poincaré) waves in a barotropic ocean over a sphere, Journal of Fluid Mechanics, 726, 123–136, 2013.

Paldor, N., Fouxon, I., Shamir, O., and Garfinkel, C. I.: The mixed Rossby–gravity wave on the spherical Earth, Quarterly Journal of the Royal Meteorological Society, 144, 1820–1830, https://doi.org/10.1002/qj.3354, https://rmets.onlinelibrary.wiley.com/doi/abs/10.1002/qj.3354, 2018.

Phillips, N. A.: Numerical integration of the primitive equations on the hemisphere, Monthly Weather Review, 87, 333–345, https://doi.org/10.1175/1520-0493(1959)087<0333:NIOTPE>2.0.CO;2, 1959.

Polvani, L. M., Scott, R., and Thomas, S.: Numerically converged solutions of the global primitive equations for testing the dynamical core of atmospheric GCMs, Monthly weather review, 132, 2539–2552, 2004.

Press, W. H., Teukolsky, S. A., Vetterling, W. T., and Flannery, B. P.: Numerical recipes 3rd edition: The art of scientific computing, Cambridge university press, 2007.

Shamir, O. and Paldor, N.: A quantitative test case for global-scale dynamical cores based on analytic wave solutions of the shallow-water equations, Quarterly Journal of the Royal Meteorological Society, 142, 2705–2714, 2016.

Thuburn, J. and Li, Y.: Numerical simulations of Rossby–Haurwitz waves, Tellus A, 52, 181–189, 2000.

Ullrich, P. A.: A global finite-element shallow-water model supporting continuous and discontinuous elements, Geoscientific Model Development, 7, 3017–3035, 2014.

Ullrich, P. A., Melvin, T., Jablonowski, C., and Staniforth, A.: A proposed baroclinic wave test case for deep-and shallow-atmosphere dynamical cores, Quarterly Journal of the Royal Meteorological Society, 140, 1590–1602, 2014.

Wheeler, M. and Kiladis, G. N.: Convectively coupled equatorial waves: Analysis of clouds and temperature in the wavenumber–frequency domain, Journal of the Atmospheric Sciences, 56, 374–399, 1999.

Williamson, D. L., Drake, J. B., Hack, J. J., Jakob, R., and Swarztrauber, P. N.: A standard test set for numerical approximations to the shallow water equations in spherical geometry, Journal of Computational Physics, 102, 211–224, https://doi.org/10.1016/S0021-9991(05)80016-6, 1992.